ELSEVIER

Contents lists available at ScienceDirect

Archives of Biochemistry and Biophysics

journal homepage: www.elsevier.com/locate/yabbi



Review article

Building on a theme: The redox hierarchy of pyridine nucleotide-disulfide oxidoreductases

Madison M. Smith, Graham R. Moran

Department of Chemistry and Biochemistry, 1068 W Sheridan Rd, Loyola University Chicago, Chicago, IL, 60660, United States



ABSTRACT

Flavin disulfide reductases (FDRs) are FAD-dependent enzymes that transmit electrons from NAD(P)H to reduce specific oxidant substrate disulfides. These enzymes have been studied extensively, most particularly the paradigm examples: glutathione reductase and thioredoxin reductase. The common, though not universal, traits of the family include a tyrosine- or phenylalanine-gated binding pocket for NAD(P) nicotinamides adjacent to the FAD isoalloxazine re-face, and a disulfide stacked against the si-face of the isoalloxazine whose dithiol form is activated for subsequent exchange reactions by a nearby histidine acting as a base. This arrangement promotes transduction of the reducing equivalents for disulfide exchange relay reactions. From an observational standpoint the proximal parallel stacking of three redox moieties induces up to three opportunities for unique charge transfer interactions (NAD(P)H FAD, NAD(P)+•FADH₂, and FAD•thiolate). In transient state, the charge transfer transitions provide discrete signals to assign reaction sequences. This review summarizes the lineage of observations for the FDR enzymes that have been extensively studied. Where applicable and in order to chart a consistent interpretation of the record, only data derived from studies that used anaerobic methods are cited. These data reveal a recurring theme for catalysis that is elaborated with specific additional functionalities for each oxidant substrate.

1. Introduction

Flavoprotein disulfide reductase FDRs are a diverse class of enzymes that catalyze the reduction of various substrates, utilizing a flavin and at least one disulfide redox center [1]. This review will confine the topic to those FDRs that utilize pyridine nucleotide and have one or more disulfide (or selenide-sulfide) pair. All of these enzymes share structural and mechanistic similarities, with each reaction utilizing electrons from a reduced nicotinamide dinucleotide substrate (NAD(P)H) to reduce a non-covalently bound flavin adenine dinucleotide (FAD). The enzymes described include (dihydro)lipoamide dehydrogenase (LipDH), glutathione reductase (GR), trypanothione reductase (TR), mycothione reductase (MR), thioredoxin reductase (TrxR), alkyl hydroperoxide reductase subunit F (AhpF), mercuric reductase (MerA), and thioredoxin/glutathione reductase (TGR). TrxR will be divided into two classes of enzymes, low MW TrxR (present in prokaryotes, archaea, and lower eukaryotes) and high MW TrxR (present in higher eukaryotes) [2].

Fig. 1 is a depiction of the redox hierarchy in the pyridine nucleotide dependent subclass of FDRs. The dimeric forms of each are shown. The yellow circles indicate the proposed catalytically relevant Cys-Cys (or Cys-Sec) pair(s) for each subunit. HMW TrxR, GR, TR, MR, TGR, LipDH, and MerA have readily apparent structural similarity and belong to Class I pyridine nucleotide-disulfide oxidoreductases, while LMW TrxR and AhpC are structurally distinct and classified as Class II. The enzymes

within the red box include those that utilize only one disulfide pair in catalysis, including LipDH, GR, TR, and low MW TrxR. Mycothione reductase (MR) also belongs in this category but currently has no reported crystal structure. Those found to utilize two catalytic disulfides (or selenide-sulfide) pairs are defined by a blue box, including high MW TrxR and AhpF. Visually, one can readily ascertain that despite possessing an additional catalytic disulfide pair, the overall structure of high MW TrxR is similar to most of the single disulfide containing enzymes. Conversely, in terms of structure, AhpF and low MW TrxR are outliers. AhpF has a TrxR-like fold but with a unique dimer interface and two appended thioredoxin (Trx)-like domains that house its second catalytic disulfide pair. Low MW TrxR has a unique structure and conformational sequence that imparts a fundamentally unique mechanism. The last two enzymes that will be discussed include MerA and TGR. MerA has been extensively characterized, however crystallization of the full-length enzyme has been challenging. In an attempt to understand this enzyme's structure, a region of the N-terminus (~100 amino acids) that has an additional third catalytic disulfide pair was removed and the truncated form was successfully crystallized and its structure solved [3-5]. Though the isolated N-terminal region's structure has been solved using NMR [6], the full-length enzyme has yet to be determined and therefore the functional placement of this portion of the structure is not known and so cannot be definitively grouped with the two or three disulfide enzymes. TGR (shown in a green box) contains

E-mail address: gmoran3@luc.edu (G.R. Moran).

^{*} Corresponding author.

three catalytically relevant disulfide (or selenide-sulfide) pairs. In terms of the redox sequence, the second pair are the terminal residues of what is thought to be the highly mobile *C*-terminus that mediates between the flavin active site and distant intra-subunit disulfides and oxidant substrates. One can readily see that both MerA and TGR share structural similarities to most of the enzymes in Class I, despite being proposed to utilize a more elaborate electron transfer sequence.

Overall, these enzymes rely on three simple chemistries to catalyze the reduction of their substrate. The first is the exchange of electrons between reduced nicotinamide and oxidized flavin, the second is flavin reduction of a proximal disulfide bond, and the third is disulfide/thiol exchange reaction(s). As stated above, all FDRs discussed in this review contain one non-covalently bound FAD per subunit. With the binding of the NAD(P)H substrate, the isoalloxazine ring of the flavin is oriented so that it is stacked parallel to the nicotinamide ring with the flavin N5 within 3-3.5 Å of the dihydronicontinamide C4: a positioning that is somewhat universal for hydride transfers of this type that was first defined for GR [7] (Fig. 2A and B). Additionally, this stacking conformation can produce charge transfer (CT) absorption, which has been useful observational handle to study these enzymes. Several of the enzymes in Class I have been reported to exhibit multiple charge transfer absorption transitions, and these have been used to assign chemistry to discrete steps and ultimately define mechanism.

The reduction of a disulfide bond to form two thiols requires two electrons and two protons (Fig. 2C). Once in the reduced form (2 (R–SH)), a nearby base can deprotonate one of the thiols to induce disulfide/thiol exchange with another disulfide, either in the disulfide electron relay or as part of an oxidant substrate [8,9]. The thiolate sulfur acts as a nucleophile attacking and crosslinking with the proximal disulfide. The remaining thiol of the initial reduced disulfide can attack this mixed disulfide, leading to disulfide/dithiol exchange. Each of these reactions is reversible and therefore the directionality/favorability of electron transfer is dictated by the redox potential of all moieties in the

electron relay and governed by the concentrations of NAD(P)H and the oxidant substrate. These factors also determine the resting reduced state of the FDR enzyme in the cellular environment and numerous FDR enzymes have been shown to accept multiple hydrides from NAD(P)H during their reductive half reactions [10–12]. Additionally, as disulfide/thiol exchange is initiated by the thiolate and thiols are only partially deprotonated at physiological pH (unperturbed Cys residues have pKa ~8), redox active disulfides are often found adjacent to residues capable of proton exchange that promote the disulfide/thiol exchange reaction. As we will discuss, for most FDR enzymes with a well characterized crystal structure, a conserved His residue is often near one or both catalytic sulfurs. Similarly, Sec residues are found in several FDR enzymes which have a pKa near 5 and will therefore be more likely to exist in the deprotonated state under physiological conditions, negating the requirement for the base [13].

FDRs are integral to cellular homeostasis and employ several complex sequences of chemical steps to function. This review will focus on the comparison of published kinetic and structural data for the pyridine nucleotide dependent subclass of FDR enzymes. As shown, the enzymes discussed here utilize various features which are conserved and/or similar to each other and, in an effort to demonstrate the progression of these characteristics, they will be discussed as a series from least to most complex in terms of the number of disulfide exchange reactions required for catalysis. While several of these enzymes have been investigated as possible drug targets, this will not be elaborated in this review. Additionally, most of the enzymes in this class have been extensively studied, however the data discussed here will be limited to those for which both anaerobic kinetic analysis and structural data are available to define mechanism. From these data a generalized chemical mechanism for the FDR enzymes will be posited.

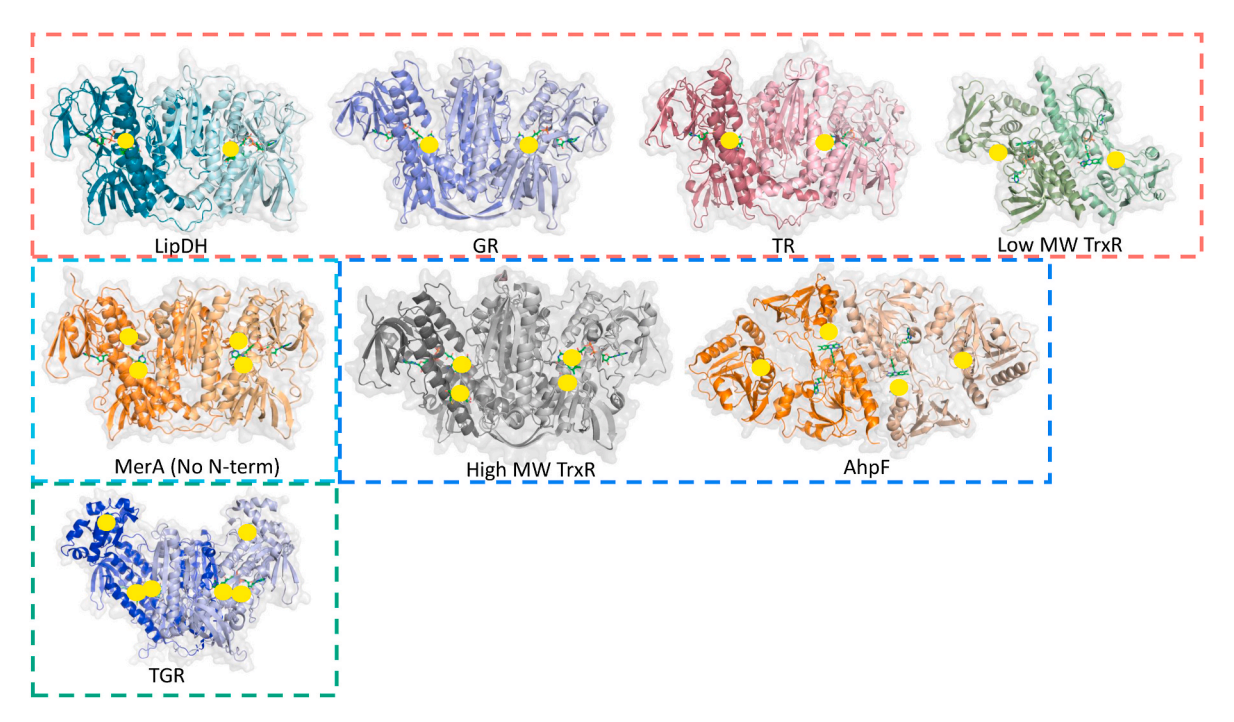


Fig. 1. X-ray Crystal Structures of Flavoprotein Disulfide Reductases. Structures display homodimers, and each catalytic disulfide pair is indicated with a yellow dot. Those encompassed by the red box possess one catalytically relevant disulfide per subunit, including (dihydro)lipoamide dehydrogenase (LipDH) (PDB 3LAD), glutathione reductase (GR) (PDB 1GET), trypanothione reductase (TR) (PDB 1NDA), and thioredoxin reductase (low MW TrxR) (PDB 1F6M). Those found within the blue box possess two catalytically relevant disulfides, including alkyl hydroperoxide reductase subunit F (AhpF) (PDB 1HYU), and thioredoxin reductase (high MW TrxR) (PDB 4J57). The teal box surrounds mercuric ion reductase (MerA) (PDB 1ZK7) and there are conflicting reports as to whether two or three disulfide pairs are required for catalysis. All published crystal structures of MerA lack a portion of the *N*-terminus (~2–95 aa), the location of the third disulfide. Thioredoxin glutathione reductase (TGR) (PDB 2 × 8C) is shown within the green box and has three disulfide pairs to catalyze the reduction of both Trx and glutathione.

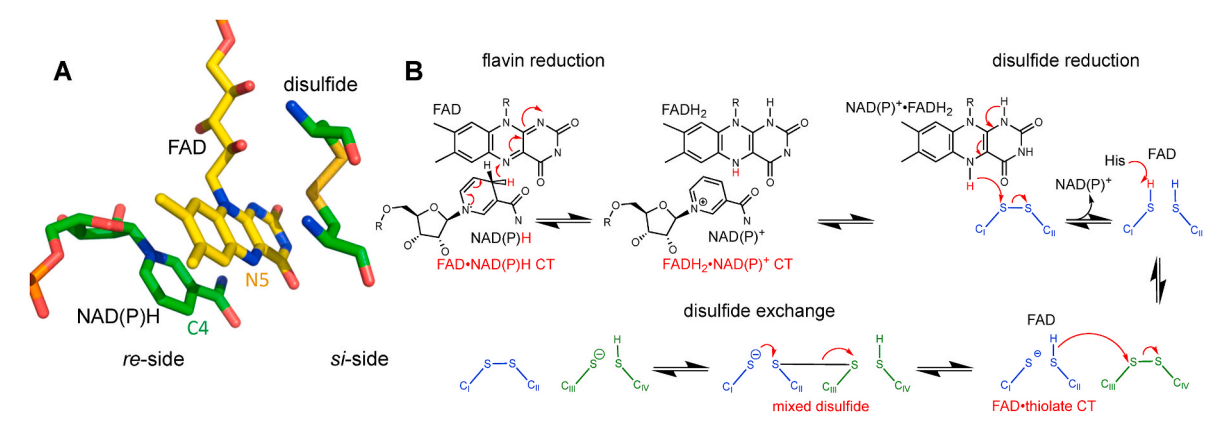


Fig. 2. The core catalytic components and fundamental chemistries of pyridine nucleotide dependent flavoprotein disulfide reductases. A. NADP(H) stacked parallel with FAD and the proximal disulfide (PDB 2X99). B. Flavin/NAD(P)H hydride exchange, disulfide reduction and disulfide exchange mechanisms depicted in series. CT indicates the potential for charge transfer absorption transitions.

2. FDRs that utilize one catalytic disulfide

The first subgroup of FDR enzymes discussed will be those found to utilize one catalytic disulfide. This redox moiety is a common feature of all Class I FDR enzymes described in this review and is located adjacent to the FAD isoalloxazine on the si face, opposite the re face binding pocket of the NAD(P)H dihydronicotinamide (as shown in Fig. 2A). As one might suspect, the electrons are proposed to transfer as hydrides from NAD(P)H to the flavin and then to the disulfide pair, where they directly or indirectly become available to reduce the oxidant substrate. For this reason, each of the FDR enzymes in this group can accept two electrons, generating the EH2 state, or four electrons, generating the fully reduced EH₄ state. In this first subgroup, we will discuss (dihydro) lipoamide dehydrogenase (LipDH), glutathione reductase (GR), mycothione reductase (MR), trypanothione reductase (TR), and bacterial thioredoxin reductase (Low MW TrxR). While there exists an extensive literature for LipDH, GR, and low MW TrxR, characterization of MR and TR is limited but due to their structure and apparent catalytic similarities to GR, these three enzymes will be also be discussed.

2.1. (dihydro)Lipoamide dehydrogenase (LipDH)

(dihydro)Lipoamide dehydrogenase was one of the first FDR enzymes to be characterized and has been studied consistently for nearly fifty years. This enzyme is a part of the α -ketoglutarate and pyruvate dehydrogenase multienzyme complex and catalyzes the oxidation of dihydrolipoamide to lipoamide, transferring electrons to NAD⁺ (Fig. 3A) [14,15]. In vivo, the reaction is driven by being coupled to the significantly negative free energy change for the oxidative decarboxylation catalyzed by the multienzyme complex. It is proposed that the substrate dihydrolipoamide will initially bind and reduce the disulfide pair proximal to the flavin generating lipoamide. The electrons will then be transferred to the flavin and then the nicotinamide to generate NADH. LipDH's have been studied in the forward and reverse direction. The enzyme has been isolated from various organisms including Sus scrofus, Azotobacter vinelandii (AzLipDH), Escherichia coli (EcLipdH), Mycobacterium tuberculosis (MtLipDH), Pseudomonas putida (PpLipDH), and Pseudomonas aeruginosa (PaLipDH) and all appear to have similar structural features and kinetic characteristics [14-19].

LipDH is a homodimer with a subunit molecular mass of 50 kDa. Each subunit is composed of four domains, the FAD-binding domain, the NAD-binding domain, the central domain, and the interface domain. Despite only having ~26% sequence identity, the fold of LipDH resembles that of GR (Fig. 1) with nearly identical active site constitution [20]. Fig. 3B depicts the LipDH active site compiled from overlaying various enzyme•ligand complexes. This image is composed of the *A. vinelandii* structure (unliganded holoenzyme) which was one of the

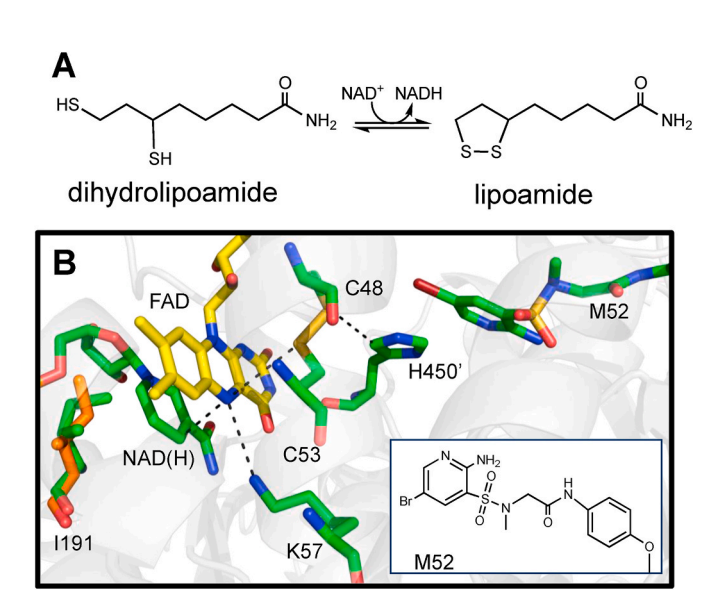


Fig. 3. LipDH catalyzed reaction and active site. A. Reaction catalyzed by LipDH. B. A composition of the binding sites and active site of LipDH generated by overlaying the AvLipDH apo (PDB 3LAD), PaLipDH•NAD(H) complex (PDB 5U8W), and MtLipDH•M52 inhibitor complex (PDB 4M52). The FAD, C48/C53 disulfide pair, K57, and I191 are from of subunit A (AvLipDH structure), while the H450 is from subunit. B. NAD(H) and the corresponding I191 residue (shown in orange) are from the PaLipDH•NAD(H) complex structure and the inhibitor molecule, M52 is from the MtLipDH•M52 complex structure.

first LipDH structures solved [17,20], the more recently determined P. aeruginosa LipDH•NAD(H) complex [15], and the M. tuberculosis LipDH•inhibitor complex [21]. One can infer the pathway of electron movement and discern the regions associated with the binding of each substrate from this aligned, ensemble structure. The NAD(H) appears to bind to the re face of the flavin, opposite to the C48/C53 disulfide and inhibitor M52 molecule (Fig. 3B). The NAD(H) nicotinamide is stacked parallel to the isoalloxazine ring of the FAD, with the C4 position at 2.9 Å from the N5 of the flavin. The catalytically relevant C48/C53 (in AvLipDH) disulfide pair is available to donate to or receive electrons from the flavin, with the C48 existing 3.9 Å from the N5 of the isoalloxazine ring. The N-methylpyridine 3-sulfonamide inhibitor molecule, M52, is shown to occupy and "block" the (dihydro)lipoamide binding site, thus it is not in close proximity to the disulfide and therefore is not a surrogate for lipoamide substrate/product binding [21]. Additionally, several researchers have theorized that a portion of the C-terminus is required to "cap" the lipoamide binding channel as several residues in

this region have been demonstrated to be catalytically relevant [18,22, 23], though there is no noticeable change in the *C*-terminus with the binding of the inhibitor molecule and no structure has yet been solved with the native substrate/product. With this composite LipDH structure one can infer the binding sites for both substrates and the pathway for electrons through the redox chain.

In 1960, Massey et al. were the first group to perform an anaerobic kinetic study of porcine LipDH [16]. When introducing reducing equivalents, either in the form of NADH, dihydrolipoamide, or dithionite, absorption spectral changes consistent with the formation of an intermediate reduced state (EH_2) were obtained. At the time, this was observed to be red in color and was therefore labeled as either a flavin semi-quinone or some other free radical state. The formation of this intermediate was determined to be the rate limiting step when observing the forward reaction (reduction by dihydrolipoamide) and its oxidation was rate limiting when monitoring the reverse reaction (reduction by NADH), suggesting that it may be related to the reduction of the disulfide. This intermediate was also detected in several more recent publications and has been assigned as a thiolate-FAD charge transfer absorption that arises from the reduction of the proximal disulfide and subsequent deprotonation of the thiol nearest the FAD [19,22,24-27]. When studying the E. coli enzyme, Hopkins et al. mutated the two cysteines of the disulfide pair (C44/C49 in EcLipDH) individually to serine [27]. Upon collecting an absorbance spectrum of the C44S variant spectrophotometric evidence consistent with the thiolate-FAD CT absorption was acquired. Additionally, when reducing the C49S variant with NADH, no charge transfer absorption accumulates. These data demonstrated that the C49 residue is responsible for the charge transfer absorption and was proposed to form a cross-link with the N5 of the flavin during disulfide reduction. The C44 residue will therefore interact with the disulfide of the lipoamide ligand. This is consistent with Fig. 3B that shows C53 (from AvLipDH) nearest the N5 of the flavin and C48 more proximal to the M52 inhibitor molecule in the putative substrate binding pocket. Utilizing the C44S EcLipDH variant, Hopkins et al. titrated the thiolate-FAD CT absorption as a function of pH and observed pKas of 2.7, 5.8, and 9.5. The pKa 2.7 was assigned to the thiol that causes FAD-thiolate charge transfer (C49), the pKa of 9.5 was assigned to the imidazole of His444 from the adjacent subunit, and the pKa of 5.8 was unassigned. Several other groups performed similar pH analyses with various forms of LipDH and obtained similar results [22,28]. When examining Fig. 3B, the His450' is a part of the C-terminal loop of the opposing subunit but is sufficiently close to interact with both the C53 (4.1 Å) and the C48 of subunit A (3.5 Å). Analogous residues will be discussed throughout this review, as FDR enzymes typically have a disulfide proximal to the flavin and a nearby acid/base residue that can serve to activate/deprotonate of one of the thiols formed with reduction of the enzyme.

In addition to the thiolate-FAD CT, several researchers also noted a weaker, long wavelength CT. In 2002, Argyrou et al. characterized this intermediate species by studying transient state kinetics of MtLipDH with NADH and Pro S NADD ([4S– 2 H]NADH) [19]. When observing reduction with excess NADH or Pro S NADD, the first spectrum to be captured in the deadtime of the instrument revealed a long wavelength charge transfer absorption centered at 670 nm. This feature was present when a fraction of the flavin was reduced and decayed concomitantly with the formation of the thiolate-FAD CT, indicative of a NAD $^+$ -FADH $_2$ charge transfer complex. The same charge transfer absorption was detected to form when introducing excess NAD $^+$ to the EH $_2$ form of the enzyme, and subsequently decayed as NADH was generated.

In addition to the previously discussed cysteine and histidine interaction, several other protein-cofactor/ligand interactions have been demonstrated to be important for the overall functionality of LipDH. In Fig. 3B, Lys57 is shown to interact with the isoalloxazine N5 (this residue is structurally equivalent to K53 of the *E. coli* enzyme) [29]. The data indicated that Lys57 is, somewhat counterintuitively, important for maintaining a low flavin reduction potential, as the authors measured a

potential of -314 mV for the wild-type enzyme and -254 mV for the K53R variant. The low flavin reduction potential for the wild-type enzyme results in the NAD(H)/FAD redox equilibrium and the high propensity for electrons to move from FADH₂ to the adjacent disulfide.

A residue has also been implicated in the regulation of the interaction of NAD(P) (H) and the FAD. For specific FDR enzymes (that will be discussed below) this residue is a Phe or Tyr and has been proposed to "block" the active site from the influence of external reductants or oxidants by undergoing a conformational change only with the binding of the NAD substrate. However, the equivalent residue in LipDH is an Ile. As shown in Fig. 3B, this residue, in both the apo and NAD(H) bound structure, would appear to exist in a similar conformation suggesting that unlike other FDR enzymes the movement of this residue may not be correlated to the binding or orientation of the nicotinamide in this enzyme. In 1991, Maeda-Yorita et al. mutated this residue to tyrosine to mimic the active site of GR [30]. While the reduction to the EH₂ state with dihydrolipoamide was not impacted, the reduction of the enzyme with NADH was slowed as was the formation of NADH. The data suggest that the gating function may not be required, but a bulky residue in this position in LipDH acts as a conformational regulator of NAD(P)H binding and electron transfer to the FAD.

Overall LipDH behaves very similarly to other enzymes in this subclass. It contains two separate substrate binding sites, with an electron transfer chain composed of a NAD, FAD, disulfide, and disulfide/thiol containing ligand. Unlike most other FDRs, electrons enter the system from the thiol state of the lipoamide substrate and the EH $_2$ (dithiol pair) intermediate state will accumulate. Electrons will then proceed to the flavin and with excess reductant, the EH $_4$ state will form. NAD $^+$ is the final electron acceptor and the flavin and NADH have similar reduction potentials, suggesting that the enzyme population will generally remain partially reduced.

2.2. Glutathione reductase (GR), trypanothione reductase (TR), and mycothione reductase (MR)

Scheme 1 shows the chemical reactions catalyzed by GR, TR, and MR. GSH is used as a signaling molecule and a reducing equivalent in cellular pathways of most organisms. MSH and Try (SH)₂ are functionally analogous to GSH but are specific to actinomycetes [31] and trypanosomatids [32], respectively. As GR has been extensively characterized and data for TR and MR is more limited, GR will be used as the model enzyme for this subclass and TR and MR will be referenced when relevant.

GR and TR are structurally similar to one another and to LipDH. Crithidia fasciculata TR (CfTR) and human GR (HsGR) share 34% sequence identity and their oxidant substrate binding cavities are compared in Fig. 4 [33,34]. Kuriyan et al. crystallized CfTR and analyzed its resemblance to HsGR [33]. It was reported that the principal differences between these two enzymes lies in the oxidant substrate binding region, as the Try (S₂) substrate binding pocket appears larger and more open to solvent relative to that for GSSG. Additionally, these authors noted that the active site of GR is comprised of a cluster of basic residues, while the TR binding pocket is found to have neutral, hydrophobic, and acidic residues, consistent with the differences in charge for GSSG versus Try (S2). In 1997, Stoll et al. performed a study attempting to modify the substrate specificity of GR [35]. Surprisingly, with the introduction of just the point mutations Ala34Glu and Arg37Trp to human GR, the variant enzyme exhibited a 700-fold preference for trypanothione over glutathione.

From crystallographic evidence, it was determined that the introduction of a Glu residue at position 34 led to the displacement of the side chain Arg347, and this conformational change along with the negative charge introduction prevented the binding of glutathione while granting the binding of Try (S₂) [35,36]. This distinct substrate specificity also explains why certain antiparasitic drugs will target TR but not inhibit GR [32,37–39]. Currently there exists no published crystal structures of

Scheme 1. Reactions catalyzed by GR, TR, and MR. A. GR will accept electrons from NADPH and reduce oxidized glutathione (GSSG) to generate two molecules of reduced glutathione (GSH). B. TR catalyzes a similar reaction, utilizing NADPH and oxidized trypanothione (Try (S₂)) to form NADP⁺ and reduced trypanothione (Try (SH)₂). C. MR has been reported to utilize either NADH or NADPH to catalyze the reduction of mycothione (MSSM) and form mycothiol (MSH).

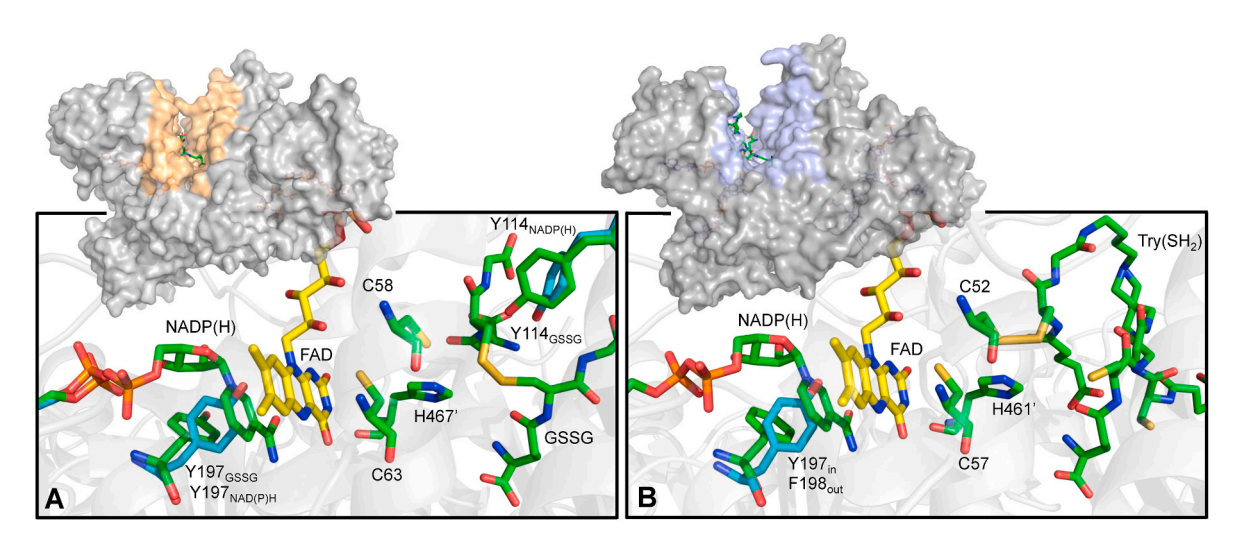


Fig. 4. Electron Relay of GR and TR. A. The HsGR•NADP(H) (PDB 3DJG) and HsGR•GSH (PDB 1GRA) structures have been overlayed. The Y197 and Y114 are displayed in two different conformations and the H467 residue of the opposite subunit is displayed to indicate its interaction with the disulfide pair. B. For comparison, a similar combined TR active site is shown. The CfTRapo (PDB 1FEC) is overlayed with TbbTR•NADP(H)•Try (SH₂) cross-linked structure (PDB 2WOW). Additionally, the F198 (of TbbTR) is shown in the out position, while the Y197 (of CfTR) is found in the in position. The H461 residue of the opposing subunit of the CfTR dimer is shown. Insets depict the oxidant substrate binding pocket of GR and TR. For A., the GR GSH complex (PDB 1GRE) is shown, with the overall dimer shown in grey and the FAD, GSH, and GSH binding pocket shown in orange. For B., the same is shown for the TR•NADP(H)•GSH/spermidine complex (PDB 1TYP), with the overall dimer shown in grey, and the FAD, NADP(H), Try (SH₂), and Try(S)₂ binding pocket shown in purple.

mycothione reductase (MR), however in 2017 a group of researchers utilized small-angle X-ray scattering in an attempt to understand the dimeric structure of *M. tuberculosis* MR (MtMR) [40]. While this structure is low resolution, they were able to demonstrate its similarity to LipDH and GR, as well as the flexibility of the NADPH-binding domain.

From Fig. 4 the electron relay of GR and TR can be discerned. For both GR and TR two different conformations of a Tyr or Phe residue near $\frac{1}{2}$

to the nicotinamide (Tyr197 or Phe198) have been reported. The movement of this residue occurs with the binding of the nicotinamide dinucleotide substrate, shifting from a position where it would potentially block access to the FAD N5 to a conformation where it stacks parallel to the nicotinamide ring (colored as cyan in Fig. 4). The movement of this residue relative to the orientation of the NADPH base appears the same for both GR and TR. Additionally, Y114 adopts two

different conformations in Fig. 4A and is thought to participate in glutathione binding. An analogous residue (Tyr109 in CfTR and Tyr110 in Trypanosoma brucei brucei TR (TbbTR)) is found in TR, however it is outside the field shown in Fig. 4B. Krauth-Siegel et al. demonstrated that mutating the Tyr197 to Ser as it is in HsGR yielded a pronounced effect on the observed kinetics of the reductive half-reaction [41]. The rate of NADPH reduction of the variant was 15-20-fold slower than that of the wild type enzyme and the extent of accumulation of the NADPH-FAD CT and NADP+-FADH2 CT were diminished. Additionally, the extent of flavin reduction was increased with the Tyr197Ser variant, indicating that while the mutation impeded NADPH binding it also raised the reduction potential of the flavin favoring accumulation of the FADH2 state. Conversely, with the mutation of the Tyr114 residue to a Leu they observe a 4-fold slower flavin reoxidation rate with GSSG as the oxidant substrate, but no influence on the reductive half-reaction. This demonstrates that the Tyr114 residue is involved in the oxidative half-reaction, conceivably contributing to the binding and/or reduction of GSSG.

Researchers have reported the accumulation of long wavelength charge transfer absorption species when studying GR and TR. When monitoring a single turnover of HsGR with 1 equivalent of NADPH and GSSG, the first spectrum collected, 8 m s post mixing, displays a CT absorption centering at 600 nm coinciding with partial flavin reduction [41]. Krauth-Siegel et al. assigned this intermediate species to that of the rapidly forming NADPH-FAD CT. Similarly, Rietveld et al. observe the formation of an analogous CT intermediate with the introduction of NADPH to the E. coli GR (EcGR) Cys47Ser variant [42]. As this form of the enzyme prevents the transfer of electrons between the FAD and the disulfide pair, these researchers observe a rapidly forming and sustained NADPH-FAD CT absorption band that accumulated with minimal flavin reduction. Opposingly, a CT absorption also centered at 600 nm accumulates when over reducing the C58S Trypanosoma cruzi TR (TcTR) variant with excess NADPH [43]. As this CT is present with fully reduced flavin, this was assigned as arising in the NADP+-FADH2 complex. Several researchers observe evidence of the NADP $^+$ -FADH $_2$ CT when monitoring the reaction of either HsGR, EcGR, or Plasmodium falciparum (PfGR) wild type enzymes, however in GR this CT absorption is centered at 670 nm [41,42,44,45]. There currently exists no data for MR consistent with the formation of either of these charge transfer complexes.

Concomitant with flavin reoxidation and proximal disulfide reduction, the NADP⁺-FADH₂ intermediate species will decay and be replaced with the thiolate-FAD charge transfer absorption and this species has been detected during the reductive half reaction for all three enzymes of this subgroup and across various species [41-44,46-48]. In EcGR, when attempting to over reduce the Cys47Ser variant enzyme with excess NADPH, no feature consistent with a thiolate-FAD CT is observed [42], indicating that the partner cysteine, Cys42 residue (Cys58 in HsGR), interacts with the GSSG substrate, and that the Cys47 (Cys63 in HsGR) residue is required for formation of the thiolate-FAD CT (consistent with residue orientation of HsGR shown in Fig. 4A) [42]. Similarly, when studying TcTR it was shown that the oxidized spectra of several Cys53 variant enzymes (either Cys53Ala or Cys53Ser) are similar to that of the EH₂ state of the wild type enzyme (i.e. resembling the thiolate-FAD CT) [43], suggesting not only that this residue is responsible for the thiolate-FAD CT but also that the deprotonated state of this thiol is favored at neutral pH in TcTR. Additionally, while the data is limited, Patel et al. noted the formation of the thiolate-FAD CT when studying MtMR and utilized its decay to monitor the enzyme's rate of reoxidation [45,46]. These researchers also measured a KIE when monitoring the formation of the thiolate-FAD CT facilitated by Pro S NADPD reduction. Not only does this confirm that the Pro S hydrogen of the dihydronicotinamide is donated to the flavin as a hydride, but it also indicates that this same hydrogen (or deuterium in the case of NADPD) is transferred to reduce the disulfide and is then abstracted generating the thiolate-FAD CT.

The active site of GR and TR have a histidine residue that is

positioned to act as base and deprotonate one of the thiols generated with the reduction of the disulfide pair. Rietveld et al. investigated this histidine's catalytic involvement by analyzing the reductive and oxidative half-reaction of the EcGR His439Ala variant [42]. Here it was demonstrated that both half-reactions were slowed, but the largest impact was the ~20-40-fold slower rate of formation of the thiolate-FAD CT. This data would suggest that this histidine is responsible for deprotonation of the thiol nearest the FAD and likely influences the redox activities of the flavin and catalytic disulfide. When studying yeast GR the spectrum of the EH2 state (or thiolate-FAD CT) was observed to titrate with pH, and resulted in measured pKa values of 4.8–5.1, 7.1–7.4, and 8.2–9.2 [28,47]. While not definitively assigned, akin to LipDH, it has been proposed that the lowest pKa reflects that of the thiol nearest the flavin and the highest is associated with the deprotonation of the histidine.

GR, TR, and MR appear to utilize an almost identical electron relay scaffold, with only slight structural variability. As each catalyzes the reduction of a disulfide bond, it is not surprising that the intermediate species are similar with variation mostly confined to the enzyme's interaction with its oxidant substrate. As the NADPH-FAD CT has typically been shown to form in the deadtime of a rapid mixing instrument, the binding of NADPH and reduction of the FAD is assumed to be rapid. As suggested by the orientation of NADP(H) in the active site of GR and TR (Fig. 4), as well as measurement of Pro S NADPD kinetic isotope effect, it can be concluded that the first step of the reaction involves the transfer of the Pro S hydride from the nicotinamide to the N5 position of the isoalloxazine ring of the FAD, resulting in the formation of a NADP⁺-FADH₂ CT absorption. Electrons are then transferred to the catalytically relevant disulfide pair and, with deprotonation of the thiol proximal to the FAD to form the characteristic thiolate-FAD CT complex. This chain of electron transfer and corresponding redox intermediates is also consistent with the observations made for the more complex FDR enzymes. However, low MW thioredoxin reductase diverges from this catalytic mechanism despite catalyzing a similar reaction (see below).

2.3. Low MW thioredoxin reductase (low TrxR) and thioredoxin (Trx)

One of the most prevalent thiol-based redox systems is composed of NADPH, thioredoxin reductase (TrxR) and thioredoxin (Trx). Reduced Trx will transfer electrons to peroxiredoxins, which will nullify reactive oxygen and nitrogen species. To maintain cellular homeostasis, TrxR will catalyze the reversible reduction of Trx with electrons derived from NADPH (Fig. 5A). This reaction is highly similar to that of GR, TR and MR, however rather than reducing a disulfide containing small molecule, Trx is a disulfide containing small protein (~12 kDa). Thioredoxin is composed of a four-stranded antiparallel beta sheet sandwiched between three alpha helices [49].

As stated above, there are two types of TrxRs, those found in prokaryotes, archaea, and lower eukaryotes labeled as low MW TrxR, and those found in higher eukaryotes labeled as high MW TrxR. As the names suggest low MW TrxR enzymes are smaller in size, typically $\sim\!35\,\mathrm{kDa}$ per subunit, while high MW TrxRs are $\sim\!55\,\mathrm{kDa}$ [1,2]. Despite both enzymes serving an equivalent purpose, mechanistically and structurally they are different. This has allowed for the pursuit of antimicrobial drugs that inhibit bacterial TrxR without cross-reactivity with the host's TrxR [49].

Bacterial TrxR (*E. coli* TrxR or EcTrxR) was originally isolated in the mid 1960s, however early attempts at characterizing its mechanism were limited as researchers were lacking information about its structure. It wasn't until 1991 that the first X-ray crystal structure of EcTrxR (PDB 1TRB) was reported, citing the significant structural differences between the, at that time, well understood LipDH and GR systems [50]. It was demonstrated that the dimeric structure and overall active site of GR and low MW TrxR are starkly different, despite possessing similar cofactor and ligand binding regions. In EcTrxR the catalytic disulfide is found on the *re* side of the flavin and buried in the protein, occupying a region where the nicotinamide binds in other enzymes in this subclass. In this

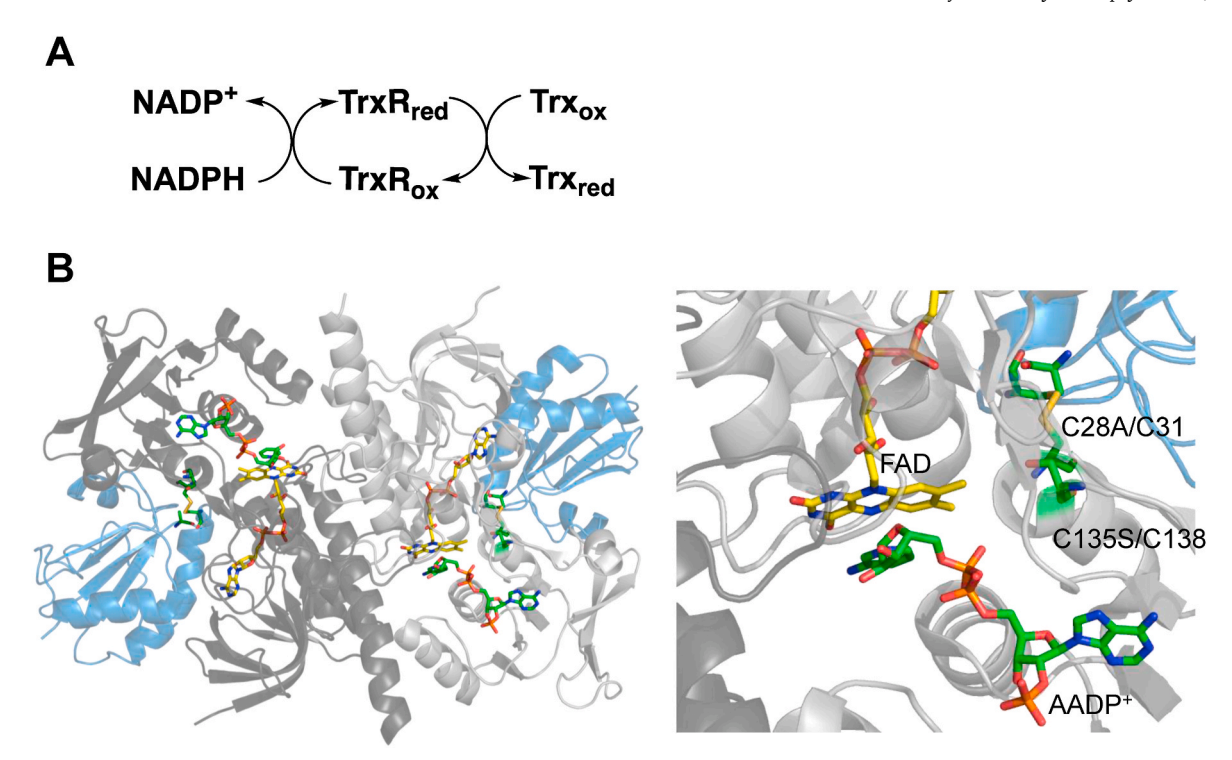


Fig. 5. Low MW TrxR. A. The reduction of thioredoxin (Trx) is catalyzed by TrxR, with electrons derived from NADPH. B. The crystal structure of dimeric EcTrxR (C135S)•EcTrx (C28S)•AADP⁺ complex is displayed (PDB 1F6M). TrxR (shown in grey) and Trx (shown in blue) are cross-linked through a disulfide bond formed between the C138 of EcTrxR and the C31 of EcTrx.

initial structure the NADPH binding domain, which was analogous to that observed in GR, was distant from the FAD molecule. Therefore, a sizeable conformational change was proposed to rotate either the NADPH or the FAD domain by $\sim\!65^\circ$, relative to one another, to allow for hydride transfer between the nicotinamide and the isoalloxazine ring [50–53]. This conformational change was thought to both correctly orient the NADPH but would also allow the catalytic disulfide to be more exposed to the solvent to facilitate Trx reduction. In 1994, Waksman

et al. reported an X-ray crystal structure of the EcTrx C138S (part of the catalytic disulfide) variant enzyme in complex with NADP(H) (PDB 1TDF) [52]. This complex was thought to be a non-catalytic conformation, as the nicotinamide ring of NAD was found $\sim\!17$ Å away from the flavin. It wasn't until 2000 that the proposed conformational change was confirmed by Lennon et al. in the capturing of the X-ray crystal structure of EcTrxR C135S variant enzyme in complex with the NADP+ analogue, 3-aminopyridine-adenine dinucleotide phosphate (AADP+)

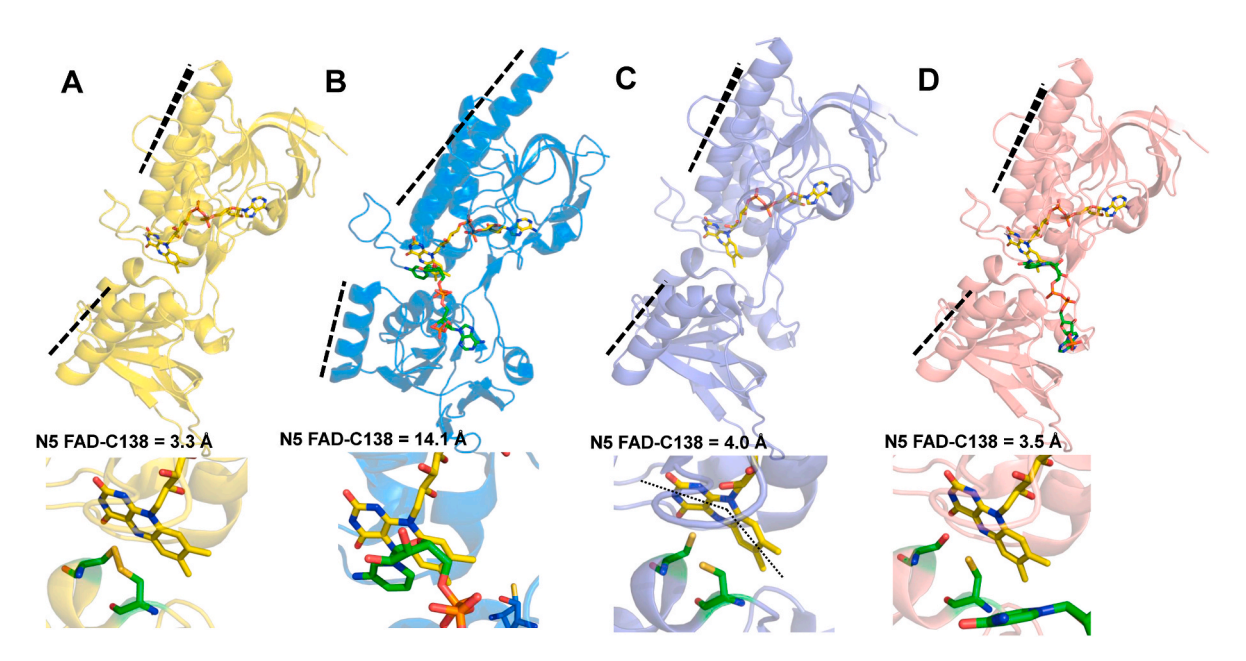


Fig. 6. Conformational changes over the course of low MW TrxR Reaction. Various *E. coli* TrxR (monomer) complexes are displayed to illustrate several redox conformations; A. EcTrxR_{unrotated} (PDB 1TDE), B. EcTrxR (C135S)•EcTrx (C28A)•AADP + rotated (PDB 1F6M), C. EcTrxR_{reduced} (PDB 1CLO) and D. EcTrxR (C138S)• NADP(H)_{unrotated} (PDB 1TDF). Each paired image depicts the FAD, C135/C138 (or S when applicable), and nicotinamide/aminopyridine (when applicable). Above the inset is a label reflecting the distance between the N5 of the FAD isoalloxazine ring and the 138 residue.

and cross-linked to EcTrx C28A variant (PDB 1F6M) [54]. In this structure the NADPH domain is shifted $\sim\!70^\circ$ allowing for the stacking of the nicotinamide and FAD isoalloxazine, while additionally orienting the catalytic disulfide near the disulfide of thioredoxin ($\sim\!14.1$ Å away from the flavin). This dimeric structure is shown in Fig. 5B. Despite capturing this conformational change, the mechanism was not initially fully understood. By combining various kinetic and structural analyzes of low MW TxrR, the pathway for electrons through the enzyme and a full catalytic mechanism was later proposed (see below).

Several captured EcTrxR crystallized states are shown in Fig. 6. The apo, oxidized enzyme found in the "unrotated" conformation is displayed in Fig. 6A, with the catalytic disulfide pair adjacent on the re face of the FAD, 3.3 Å away from the N5 of the isoalloxazine ring (PDB 1TDE) [52]. Fig. 6B depicts the "rotated" conformation of the TrxR (C135S). Trx (C28A)•AADP⁺ complex (PDB 1F6M) [54]. Here the NADP(H) nicotinamide is stacked on the re face of the FAD, with the C138 residue located 14.1 Å from the flavin. The four-electron reduced state is displayed in Fig. 6C, which contains a flavin isoalloxazine bent by 34° signifying the FADH2 state and two thiols at position C135/C138 (PDB 1CL0) [55]. Given that sodium dithionite was the reductant used to over reduce the enzyme while soaking the crystals and it is NADPH binding that is proposed to induce the rotation, it is not surprising that the enzyme is found to be in the "unrotated" conformation. Fig. 6D reflects the TrxR (C138S)•NADP(H) complex discussed previously (PDB 1TDF) [52] where the enzyme exists in the "unrotated" conformation, with the C135/S138 nearest the flavin and the nicotinamide appearing to be pointed out of the active site (\sim 17 Å from the FAD). While some have suggested that this is a non-catalytic conformation, it could also be argued that this captured an intermediate orientation consistent with either NADPH association or NADP+ dissociation.

In 1964, Moore et al. was one of the first to isolate and characterize bacterial TrxR under anaerobic conditions [56]. Three years later, Zanetti et al. spectrophotometrically tracked the reduction of bacterial TrxR with NADPH, dithionite, and NADH [57]. They determined that four electrons were required per FAD to fully reduce the flavin, establishing the existence of a redox moiety in addition to the flavin. Also, they reported accumulation of a charge transfer band that centered at 600 nm and attributed this to the interaction between reduced flavin and NADP⁺, as it was not observed with dithionite reduction and is eliminated with the introduction of DPNase (which will hydrolyze only NADP⁺ form). However, these researchers, along with other early reports, do not see any evidence of a broadly absorbing thiolate-FAD charge transfer, which has been observed in all other enzymes in the one catalytic disulfide subclass of FDR enzymes [57,58].

An anaerobic transient state study was performed in 1997 by Lennon et al. [59]. These researchers document tri-phasic kinetic traces when the enzyme was mixed with NADPH. The first phase was assigned as the formation of an NADPH-FAD CT complex (with absorbance centered at 560 nm), which forms in the dead time of the instrument and accumulate maximally with minimal flavin reduction. The formation of this CT feature was diminished as the enzyme reduced in the presence of high concentrations of NADP+, consistent with the assignment. The second phase has been assigned as flavin reduction followed by a slower third phase which these researchers label as the formation of an NADP⁺-FADH₂ CT complex (with absorption centered at 590 nm, but monitored at 690 nm). And in a converse manner, the inclusion of excess NADPH diminished CT absorption suggesting that NADPH can compete with the bound NADP⁺. These observations are entwined with necessary large and potentially stochastic conformational changes and so may not follow a clearly defined catalytic sequence as seen with the high molecular weight FDR enzymes.

When characterizing the reductive half-reaction of the C138S and C135S variant enzymes these researchers noted that the C135S displays kinetic characteristics that are very similar to the wild-type enzyme. This indicated that the third phase was not related to the slow reduction of the flavin by a second equivalent of NADPH as electrons move to the

adjacent disulfide. In contrast, the accumulation of both charge transfer species was significantly diminished when monitoring the C138S variant enzyme's reductive half-reaction. The authors attribute this to the serine 138 residue perturbing the equilibrium of "rotated" vs "unrotated" conformers, therefore altering the binding of NADPH (discussed further below). It is unknown whether this variant prevents the binding of NADPH or impacts the conformational change (or both) but these results may explain the state captured in Fig. 6D, where NADP(H) is depicted bound to the enzyme but in a conformation which would not result in NADP(H)-FAD (H₂) CT absorption.

Over the course of nearly sixty years of investigation, several mechanisms have been proposed for the EcTrxR catalyzed reduction of Trx. While researchers have consistently acknowledged that low MW TrxR greatly differs from that of other one disulfide containing enzymes. The lack of structural data for the major fraction of this time and the complexity of data observed made defining a discrete catalytic mechanism challenging. However, the Williams lab have proposed one line of thinking that is consistent with most kinetic and structural data [51,59, 60], these researchers postulate that the enzyme exists in an equilibrium between the "unrotated" (Fig. 6A) and "rotated" (Fig. 6B) conformation and that the "unrotated" conformation is favored to crystallize. Additionally, their findings demonstrated that during catalysis the enzyme cycles between the four and two-electron reduced states and argue that the enzymatic sequence begins with the FAD-(SH)2 state with the enzyme in the "unrotated" conformation (similar to Fig. 6C, but without reduced flavin). Upon the binding of NADPH, the conformational change is induced and reflected in the formation of the NADPH-FAD CT, prior to flavin reduction. Once in the "rotated" state, the catalytic thiol pair is available to transfer electrons onto oxidized Trx. Concomitantly, flavin reduction will occur and the second charge transfer (NADP⁺-FADH₂) is formed. When lacking oxidant and at lower NADPH concentrations, this NADP+-FADH2 CT species is sustained. However, at higher NADPH concentrations (~30-fold the enzyme concentration) this long wavelength characteristic will decay (likely a result of NADPH binding competition). The enzyme must then return to the "unrotated" conformation to regenerate the FAD-SH2 state to complete the catalytic cycle. They have postulated that this final conformational change, which returns the enzyme to the "unrotated" state, is not dictated by NADP+ dissociation, however, the direct data to support this claim is limited. Fig. 6D may therefore reflect a different binding orientation of NADP(H) which is utilized when the enzyme is in the "unrotated" conformation.

These authors suggest that the three phases of flavin reduction observed under transient state conditions is a result of the presence of both the "unrotated" and "rotated" conformations at all times such that observational delineation of species is unlikely. Thus, while it seems that this rotation can be favored with the binding of NADP(H), this conformational change will be occurring regardless of the ligands bound. This leads to blending of events and offers explanation for why each phase cannot be attributed to the accumulation of a single intermediate state. This would also account for rapid NADPH-FAD CT formation and flavin reduction when NADPH binds to the pre-"rotated" form (as this state forms within the dead time of the stopped-flow instrument (less than 4 m s)), but when binding to the "unrotated" form, its formation will be limited by the conformational change and result in trailing formation of the charge transfer and subsequent flavin reduction. They argue that the wild-type and C135S variant stabilize the "rotated" conformation, and conversely the C138S variant stabilizes the "unrotated" conformation and consequently exhibits minimal nicotinamide induced CT species and reduced flavin states. Additionally, Trx has been proposed to stabilize the "rotated" conformation. Although the conformational change was structurally characterized relatively recently, no additional kinetic data has been introduced to advance the understanding of low MW TrxR's catalytic mechanism.

3. Systems composed of two or more catalytic disulfides

Despite possessing machinery that is highly similar to the enzymes listed above, while also catalyzing similar reactions, the enzymes in this section have added regulatory and structural features. The enzymes described below utilize at least two catalytic disulfide pairs (sometimes including selenide-sulfide pairs) to catalyze the reduction of their oxidant substrate. Additionally, these enzymes are observed (or sometimes speculated) to utilize specific conformational states to bind their oxidant substrates. This section will include a synopsis of data for alkyl hydroperoxide reductase subunit F (AhpF), high MW thioredoxin reductase (TrxR), and mercuric ion reductase (MerA). High MW TrxR has been extensively studied, however the literature account for AhpF and MerA data is limited. As a result, portions of their catalytic mechanisms are sometimes inferred from their similarities to other FDR enzymes.

3.1. Alkyl hydroperoxide reductase subunit F (AhpF)

The peroxiredoxin reductase system is ubiquitous and, along with catalase, degrades endogenous hydrogen peroxide [49,61]. While some bacteria such as *Helicobacter pylori* and *Mycobacterium tuberculosis* rely exclusively on the Trx system to donate electrons to peroxiredoxin, several bacteria also possess alkyl hydroperoxide reductase subunit F (AhpF) [49,61–65]. First identified in 1989, *Salmonella typhimurium* AhpF (StAhpF) was shown to be necessary for cellular survival [66,67]. Similar to the TrxR/Trx system, AhpF was shown to catalyze the regeneration of the reduced form of the peroxiredoxin alkyl hydroperoxide reductase subunit C (AhpC), with electrons obtained from NAD(P) H [61,68,69]. Reduced AhpC will in turn catalyze the degradation of hydrogen peroxide, alkyl hydroperoxide, or reactive nitrogen species [62,67,68]. Most AhpF share ~34–40% sequence identity with bacterial TrxR, possessing a C-terminal region that is structurally highly similar to EcTrxR [69]. Additionally, AhpF possess a 200 amino acid N-terminal region.

Fig. 7 compares the structure of *E. coli* TrxR [52] with that of StAhpF [70] and *E. coli* AhpF (EcAhpF) [71]. The TrxR-like "trunk" of all three enzymes contains the NAD(P)H binding site, the FAD, and one of the catalytic disulfide centers (C345/C348 of StAhpF and EcAhpF). Appended to the TrxR-like "trunk" is the *N*-terminal region formed from two contiguous Trx-like folds, which contain the second catalytic disulfide pair (C129/C132 of StAhpF and EcAhpF). This *N*-terminal domain is proposed to be responsible for the reduction of the AhpC disulfide pair (C47/C132 of *E. coli* AhpC [71] and C46/C165 of *S. typhimurium* AhpC [63]) (discussed below). Additionally, there exists a linker region (wheat colored) composed of the amino acid residues 197–209. Fig. 7B displays the first structure of StAhpF solved [70]. When comparing this dimer to that of EcAhpF (Fig. 7C) [71], one can see

that while both contain identical domains, the conformation of the Trx-like N-terminal domains are different. Fig. 7B displays a compact conformation, with the N-terminal domain swung inwards placing the catalytic disulfide pairs in greater proximity to one another (\sim 33 Å). Fig. 7C depicts the apo EcAhpF structure captured in 2014 revealing the "elongated" conformation and is argued to be more optimal for electron transfer from the catalytic disulfide pair of the N-terminal domain to the disulfide of AhpC.

In 2015, while attempting to determine the NADH bound structure of EcAhpF, the Li Calzi et al. reported a small conformational change with the binding of the ligand [72]. The Low MW TrxR-like trunk appears unchanged, but the N-terminal domain is shifted inward. The same conformational shift of the N-terminal domain was observed in the EcAhpF•NAD+ complex (PDB 4YKG) (not shown) and therefore this conformational change has been proposed to be related to the binding of NAD molecules in the C-terminal domain. Despite being bound to the predicted NADH binding site, the nicotinamide ring (of either the NADH or NAD⁺ complex structure) appears to be ~14–17 Å from the FAD isoalloxazine ring. This orientation is highly similar to that of the NADP (H) molecule in the EcTrxR (C138S)•NADP(H) complex shown in Fig. 6D, and therefore the orientation of the nicotinamide in all three enzyme complexes may depict a catalytically relevant state. Due to its structural similarity to low MW TrxR, several researchers have suggested that AhpF may also shift between a "rotated" and "unrotated" conformation, with the NADH domain proposed to twist ~65-70°, stacking the nicotinamide and isoalloxazine rings and displacing the first catalytic disulfide center away from the FAD and nearer to the second disulfide pair [72,73]. While this "rotated' conformation has yet to be captured with any form of AhpF, it was computationally modeled using the established EcTrxR conformational change [73], and this state was often incorporated when proposing the enzyme's chemical mechanism.

During the mid-1990s, several research groups purified and assessed the function of what they label as an NADH oxidase/alkyl hydroperoxide reductase flavoprotein from *Amphibacillus xylanus* (AxAhpF) [64,74,75]. This enzyme was shown to degrade alkyl hydroperoxide in the presence of Salmonella typhimurium AhpC. While lacking structural evidence, they were able to determine that this enzyme possess three redox active centers as six electrons where acquired for it to become fully reduced [74,75]. However, they did not describe accumulation of a species indicative of a thiolate-FAD CT absorption and suggested that, like low MW TrxR, the FAD-(SH)₂ state (where the most proximal disulfide is reduced and the flavin is oxidized) may not favor the "rotated" conformation which will place the first thiol pair near the flavin. While not discretely mentioned one could theorize that this observation may be related to a possible change in the redox state of the flavin as the conformational rotation occurs with the binding of the NAD. When titrating NADH to the enzyme, Ohnishi et al. reported the accumulation

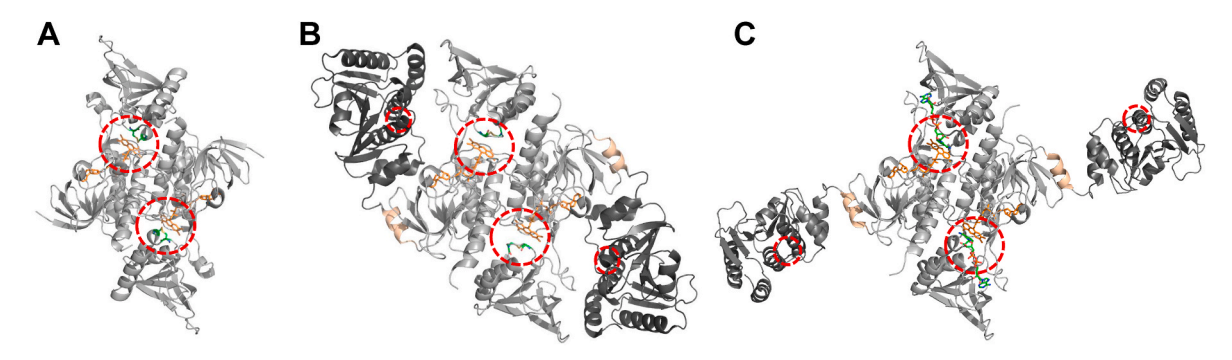


Fig. 7. Comparison of AhpF and low MW TrxR. A. The dimeric structure of EcTrxR (PDB 1TDE), B. StAhpF (PDB 1HYU), and C. EcAhpF (PDB 4O5Q) are displayed. For each structure the TrxR region is shown in light grey, the FADs are colored orange, and the catalytically relevant cysteines are encircled. B and C depict the compacted and elongated conformation of AhpF, respectively. Within these two structures, the linker regions are wheat colored and the Trx-like regions, containing the second disulfide pair, are shown in dark grey.

of an FADH₂-NAD⁺ CT absorption feature extending beyond 800 nm. However, as no time-dependent data was provided, it is difficult to discreetly assign the events observed to a specific intermediate state.

In pseudo-first order kinetic experiments Niimura et al. obtained multiphasic data when monitoring AxAhpF reductive half-reaction with excess NADH [75]. Two equivalents of NADH/mol of flavin are consumed at an observed rate of \sim 55–200 s⁻¹, while a third equivalent is consumed at a slower rate of $\sim 0.35 \, \mathrm{s}^{-1}$, as the flavin remains reduced. These phases are attributed to rapid reduction of the flavin and generation of the EH4 state, followed by the slower reduction of the second disulfide and formation of the EH₆ state. It is possible that the final phase of NADH consumption is limited by the rate of the conformational compaction that is necessary to reduce the distal disulfide. While studying various mutant enzymes Niimura et al. demonstrated that the catalytic disulfide pair (C337/C340 in AxAhpF), equivalent to the catalytic disulfide of EcTrxR, is necessary for the rapid reduction of AhpC and degradation of alkyl hydroperoxide [75]. When analyzing the reductive half-reaction of the C337S/C340S variant of AxAhpF, they noted a similar fast flavin reduction/NADH oxidation phase which titrated to a limit of 285 s⁻¹ ($K_{NADH} \sim 110 \mu M$). However, in this phase only one equivalent of NADH was consumed per mole of flavin. This indicated that without the C337/C340 residues, the enzyme could only accept two electrons and was unable to efficiently transfer electrons to the N-terminal disulfide pair (C128/C131).

A similar study was performed by Calzi et al. when attempting to characterize AhpF enzyme from *Salmonella typhimurium* (StAhpF) [76]. By studying various mutant enzymes that lacked one of the disulfide pairs, and comparing their fluorescence, absorbance, circular dichroism spectra, and partially characterizing their reductive half-reactions and reoxidation via AhpC, they were able to demonstrate that this enzyme behaves similarly to that of AxAhpF. Both groups note unchanging oxidase and transhydrogenase activities with all variants, while DTNB and AhpC reduction are significantly diminished with any variant lacking one or both of the catalytic disulfides [75,76].

In early April of 2000, Poole et al. published two manuscripts focused on the function of the *N*-terminal disulfide pair of StAhpF [77,78]. The first crystal structures became available in 2001, so this group utilized structural modeling to anticipate the secondary structure of either region and went on to isolate both domains and analyze them independently [78]. They established that each isolated domain folds properly independent of one another and when combined will retain the enzyme's function, though the peroxidase activity was decreased by ~260-fold when fragmented. The significant diminishment of the peroxidase activity was attributed to the slowing of the transfer of electrons between the C-terminal (residues 208-521) and N-terminal (residues 1-202) fragments. Additionally, attachment of a fluorophore to the C165 of the AhpC revealed that the N-terminal fragment alone was responsible for the electron transfer to AhpC. This group also fused the N-terminal 207 amino acid residues of StAhpF to EcTrxR [77]. This protein was revealed to possess both AhpC reductase and Trx reductase activities, as well as accumulate the same partially reduced states suggesting that electrons move through the fused enzyme in the same fashion. For this chimeric form the k_{cat} based on AhpC reduction was ~3-4-fold slower and the Trx reductase activity was nearly identical to that of EcTrxR. This indicated that the additional N-terminal appended region does not block access to the Trx disulfides nor impact the rotational conformational change required for catalysis.

In 2007, the Poole group re-evaluated their analyses of the StAhpF enzyme incorporating evidence from a crystal structure of the StAhpF (PBD 1HYU) [70] and proposed a catalytic mechanism and electron transport pathway for AhpF [73]. This group isolated various single and double Cys to Ser variants to alter the catalytic disulfides of both StAhpF and StAhpC to measure the cysteine reactivity and protein-protein interaction. The reactivity determination of several variant and cross-linked protein forms suggests that the C348 of the first catalytic disulfide of StAhpF will act as a nucleophile, initiating the electron relay

to the C129/C132 disulfide of the N-terminal region (Figs. 2 and 7). Furthermore, the C129 residue is argued to then attack the C165 of the C46/C165 catalytic disulfide of StAhpC. Their data suggested the need for significant domain movements to permit electrons to transfer and utilized the StAhpF X-ray crystal structure and the rotated cross-linked structure of the EcTrxR.Trx complex (PDB 1F6M) to model the pathway of proposed conformations that occur over the course of AhpF's reduction of AhpC [54,73]. The mechanism proposed included the existence of two catalytic conformations, one allowing the first catalytic disulfide pair (C345/C348) to access the flavin, and one exposing this moiety to the solvent while stacking the nicotinamide ring against the isoalloxazine ring of the FAD. When modeling this domain shift, as expected, the magnitude and direction was highly similar to that of EcTrxR, with the NAD domain rotating 57°. Additionally, they modeled the 100° rotation and 8 Å shift of the *N*-terminal region concomitantly. In this "rotated" and "compacted" model of AhpF, the second disulfide pair (C129/C132) is nearer to the first disulfide pair (C345/C348) and the transfer of electrons between these redox groups was made more likely (although the distance was not indicated). This group's proposed mechanism agrees both with past kinetic studies and with the more discovered EcAhpF "elongated" conformation EcAhpF•NAD(H) complex structures [71,72]. As later proposed by Kamariah et al. the AhpF enzyme likely shifts between the "rotated" and "unrotated" conformation to swap the positioning of the nicotinamide dinucleotide and the first disulfide pair relative to the flavin (identical to that of EcTrxR), but also possess various conformations of the N-terminal region which will dictate the second disulfide pairs interaction with either the first disulfide pair or with the AhpC substrate [72]. Despite obtaining structures of EcAhpF bound to NAD⁺ and bound to NADH, the twisted conformation of AhpF has not been observed. AhpF has been demonstrated to utilize equivalent redox machinery to that of low MW TrxR, and similarly the sequence catalytically relevant conformational changes is not fully understood and for both may instead rely on stochastic movements within an overall energetically favored reaction.

3.2. High MW thioredoxin reductase (high TrxR)

Another FDR enzyme that has been demonstrated to utilize a chain of three redox centers is high MW TrxR. Originally isolated from rat liver in the late 1960s, this ~55 kDa protein has also been identified in various organisms including *Plasmodium falciparum* (Pf), *Drosophila melanogaster* (Dm), and several mammals [10,79–83]. In mammals, two types of TrxRs have been documented: cytosolic TrxR1s and mitochondrial TrxR2s [49,84–86]. Identical in function to low MW TrxRs, these enzymes are responsible for the regeneration of reduced Trx, with electrons from NADPH [87]. The structure and mechanism of high MW TrxR would appear to be more closely related to GR, TR, MR and LipDH.

Fig. 8 compares the structures and electron relay of human GR [88] and high MW TrxR [89,90], which share 44% sequence identity [87,91]. One can see that these two enzymes are structurally very similar, with high MW TrxR having an additional C-terminal extension of ~20-45 amino acids, [87]. These residues form a C-terminal loop that interacts with the opposing subunits' FAD active site. When comparing the active site of HsGR and HsTrxR one can see that the FAD and the (first) catalytic disulfide pair (C63/C58 of HsGR and C64/C59 of rat TrxR (RnTrxR)) exist in near identical conformations (Fig. 8B). Interestingly, all residues seen to directly interact with the glutathione substrate of GR are conserved in TrxR [90]. When overlaying these two active sites, it would appear that the sulfurs of the reduced product of GR (2 GSH molecules) are similarly located when compared to the sulfurs of the proposed catalytically relevant residues (originally C497/U498) in the C-terminal loop of mammalian TrxR. This suggests that the pathway of electron transfer through GR and high MW TrxR is likely very similar, but rather than electrons being transferred from the cysteine pair adjacent to the FAD and then to the small molecule oxidant substrate, the C-terminal disulfide (or selenide-sulfide of the mammalian enzyme) acts

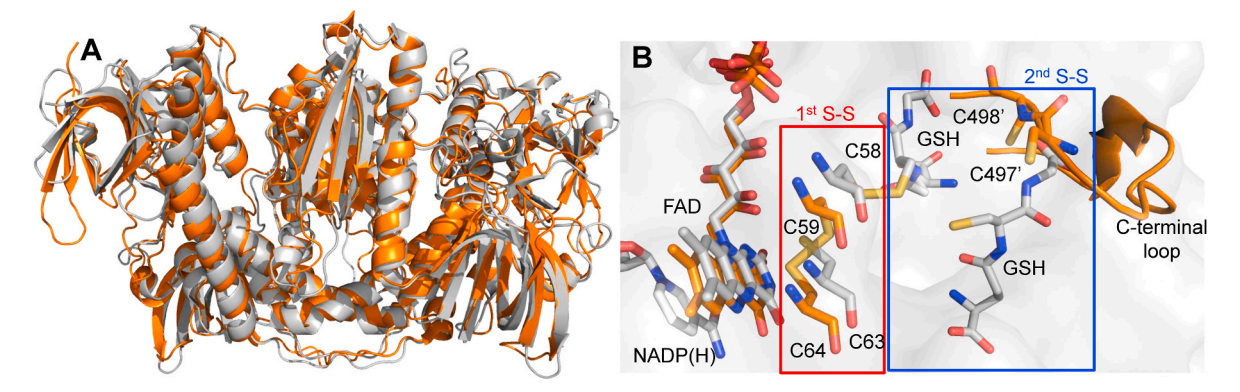


Fig. 8. The structural similarities of high MW TrxR and GR. A. The overall dimeric structure of HsTrxR (orange) (PDB 2J3N) and HsGR (grey) (PDB 1GRE) are compared, highlighting their almost identical tertiary structure. In B, the active site of several enzymes have been overlayed (RnTrxR (U498C)•NADP(H) shown in orange; PDB 1H6V) (HsGR•GSH (PDB 1GRE) and HsGR•NADP(H) (PDB 1GRB) shown in grey). The RnTrxR•NADP(H) complex was utilized as the source of second catalytic disulfide pair (found on the C-terminal loop).

as the electron recipient. The *C*-terminal loop is often unresolved in crystal structures and therefore is thought to have mobility. This dynamic behavior is proposed to be necessary both to extend to the enzymes surface to allow for electron transfer to Trx and to block the first thiol pair from reacting with other oxidants. While researchers captured NADP(H) bound in HsGR, for the RnTrxR (U498C)•NADP(H) complex the nicotinamide was out of the active site and distant from the flavin isoalloxazine [90]. High MW TrxR also has what appears to be a conserved gating tyrosine residue, Y200 (not shown, but analogous to Y197 described for HsGR) (Fig. 4). Similarly, high MW TrxR possess a Tyr residue (Y145 of PfTrxR and Y116 of HsTrxR) [92] (not shown) which were found to adopt the same conformation as the Y114 of HsGR (Fig. 4A). As discussed above, with GR this Tyr has been proposed to be related to GSSG substrate binding and may also influence the conformation of the *C*-terminal redox pair in high MW TrxR.

Fig. 9 displays the HsTrxR•Trx [93] and PfTrxR•Trx complexes [92]. In both complexes the *C*-terminal C498 of HsTrxR or C540 of PfTrxR are

cross-linked to the C32 of HsTrx or the C30 of PfTrx, demonstrating the *C*-terminal loop oriented out of active site and capturing the presumed intermediate state that occurs during disulfide/thiol exchange.

Interestingly, while the *C*-terminal catalytic residues of both enzymes exist in a similar conformation (insets of Fig. 9), the cysteine(s) or selenocysteine residues are found in a GCUG motif in mammalian TrxR but as a GCxxxxCG motif in PfTrxR [92]. Additionally, TrxRs from *Apicomplexa* and some algae have been shown to retain a conserved H438 residue adjacent to the C535 residue (3.6 Å) in the PfTrxR•Trx complex (Fig. 9B inset). However, no similar residue exists in mammalian TrxR enzymes. While no investigation of H438 has been performed, it has been proposed that its functions to deprotonate the C535 residue to promote disulfide/thiol exchange with the oxidant substrate [92]. Though the mammalian enzyme is lacking this His residue, the selenocysteine (at position 498) is expected to have a significantly lower pka (~5) compared to a cysteine (pKa ~8) [94] possibly negating the requirement for the base in disulfide exchange [94]. In addition, a small

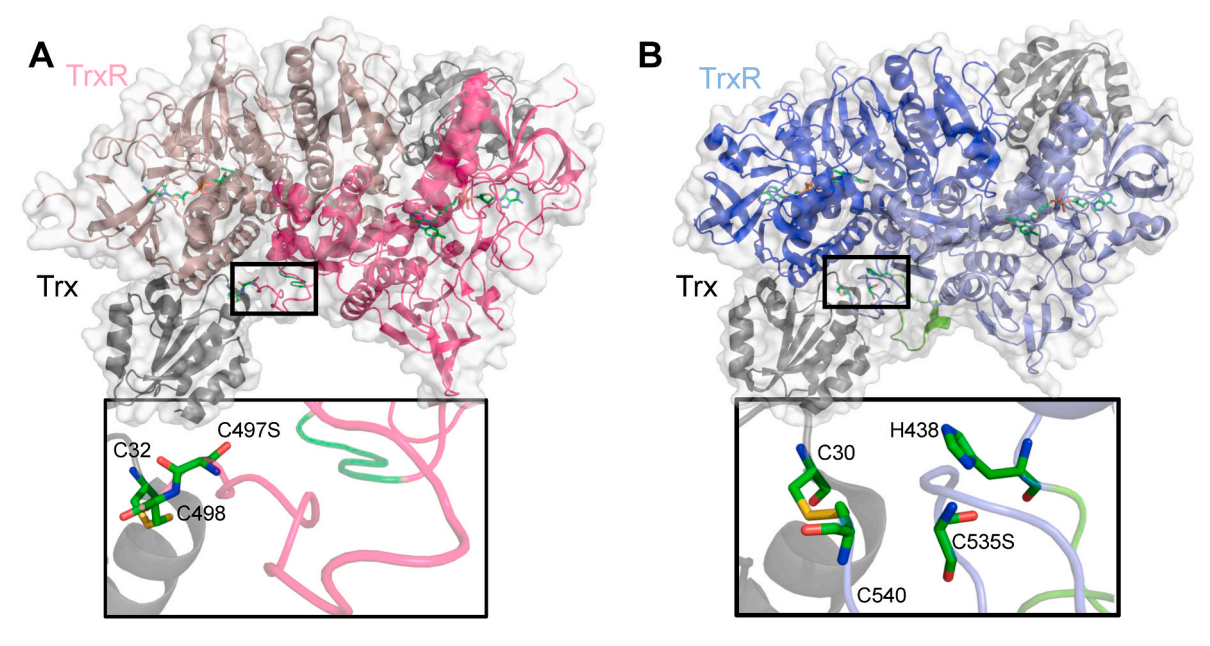


Fig. 9. Highlighting structural differences between two high MW TrxRs. A. The dimer of the HsTrxR •Trx (PDB 3QFB) complex is shown. The same is reflected in B but for the PfTrxR•Trx (PDB 4J56) complex. For both structures the flavins are shown in yellow, the TrxR portion is shown in the darker color with the Trx in the lighter color, and the loops being compared are highlighted in bright green. For the HsTrxR this loop reflects residues 415–419, while the larger loop of PfTrxR includes residues 438–456. The black squares surround the area displayed within the inset. This depicts the relevant *C*-terminal residues of the TrxR enzymes cross-linked to a Cys of Trx. Two of the *C*-terminal TrxR residues were mutated to Ser to prevent the breakage of the cross-link disulfide bond; additionally, the seleno-Cys 498 of the HsTrxR has been mutated to a Cys prior to crystallization.

loop in the *C*-terminal region, bridging between a short helix and a β -strand, is found to be different when comparing mammalian TrxR and PfTrxR. This loop includes residues 438–456 of PfTrxR, while the same loop of HsTrxR has 14 less residues, comprised only of residues 415–419 (both shown in green) [92]. Additionally, a deletion of this loop in the PfTrxR enzyme results in \sim 7-fold weaker K_M when measuring the steady state kinetics with Trx as the oxidating substrate [92]. As seen in Fig. 9, the larger loop of PfTrxR not only contains the H438 which is thought to be catalytically relevant, but it also occupies a gap formed by the PfTrxR \bullet Trx complex that remains exposed in the mammalian complex.

While this enzyme was identified and isolated from several mammals in the late 1960s to early 1970s, attempts at discerning the enzymes mechanism were not made until the late 1990s. Arscott et al. initially characterized the reduction of HsTrxR utilizing anaerobic techniques and obtained kinetic data analogous to those of LipDH and GR [95]. Upon the introduction of dithionite, they saw the formation of a thiolate-FAD CT absorption followed by secondary flavin reduction. To obtain the maximal accumulation of the thiolate-FAD CT, the enzyme required ~2-3 equivalents of dithionite and full flavin reduction was not achieved until ~3-4 equivalents of dithionite were introduced, hinting at the involvement of the second selenide-sulfide pair. With the introduction of five-fold excess of NADPH, while monitoring the reductive half-reaction for ~400 ms, the authors report evidence of the formation of the NADPH-FAD CT and NADP+-FADH2 CT absorptions, prior to thiolate-FAD CT accumulation. The TrxR enzymes isolated from P. falciparum [83,96] and D. melanogaster [10] behaved similarly.

Utilizing site-directed mutagenesis and heterologous expression, the Muller and Williams groups attempted to characterize the direct role of the proposed catalytic cysteines in PfTrxR and understand how they relate to the intermediate reduced species that accumulate [2,83,96,97]. With the introduction of an alanine or a serine to replace either cysteine of the disulfide pair adjacent to the flavin (C88/C93) a total loss of activity was observed, suggesting catalytic relevance [83]. When analyzing the reductive half-reaction, both C88A and C93A variants displayed partial flavin reduction and weak thiolate-FAD CT absorption, suggesting that both residues likely influence the redox potential of the flavin and both may contribute to the thiolate charge transfer band. It was proposed that deprotonation of C93 leads to the formation of the thiolate-FAD CT and that this residue's orientation and/or protonation state may be influenced by the C88 residue. The crystal structure revealed the C93 residue of PfTrxR to be nearer to the flavin, suggesting that its deprotonation results in the formation of the thiolate-FAD CT absorption [98]. The H509 residue was mutated to Gln and Ala and these enzymes demonstrated a 95% and 97% loss of activity, respectively [83]. Despite at the time lacking structural understanding, this residue was later recognized to be positioned similarly to the H467' of HsGR (found on the C-terminal loop) where it functions as a catalytic base to promote reactivity of the first thiol pair by generating a thiolate. Additionally, this group went on to mutate the C-terminal cysteines and characterize their involvement in the Trx reduction/TrxR oxidative half-reaction [97]. The alteration of this second redox center did not alter the reductive half-reaction. They demonstrated that the C540A variant requires only ~2 equivalents of dithionite to observe complete flavin reduction, consistent with the nullification of one redox active moiety. Additionally, by tracking the release of TNB after reducing a C540-TNB tagged C535A variant enzyme with equivalents of NADPH they determined that one equivalent of TNB is released prior to the formation of the thiolate-FAD CT. These authors suggest that this demonstrates that the electrons from the first reducing equivalent accumulate on the C-terminal redox center, indicating that this disulfide has the highest reduction potential of the electron relay [2,96,97]. During the same period, the Holmgren lab also investigated the functionality of the C-terminal redox active center of mammalian TrxR and were specifically interested in understanding the role of the selenocysteine [94,99]. When mutating the U498 to Cys, they report a 100-fold decrease in k_{cat} when monitoring the reduction of Trx [99]. When

replacing this residue with a Ser or cleaving off the last two residues of the *C*-terminus (U498 and G499), the enzyme was rendered inactive, but the reductive half-reaction with respect to the flavin and adjacent disulfide remained operative.

Later, Bauer et al. characterized the TrxR enzyme from D. melanogaster (DmTrxR) [10]. Though highly similar to mammalian and PfTrxR, it possesses two adjacent catalytic Cys residues that form its second disulfide pair (unlike the GCUG motif of mammalian TrxR and the GCxxxxCG motif of PfTrxR). While characterizing the transient state reductive and oxidative half-reactions of DmTrxR, this group reported a triphasic process, for which they labeled as the delineation between the accumulation of various reduced states including the NADP+-FADH2 CT complex, the reduction of the first disulfide and formation of the thiolate-FAD CT, and reduction of the C-terminal disulfide. Additionally, similar to other high MW TrxR enzymes, the fully reduced (or EH₆) state, in which the FAD is reduced, accumulates slowly and minimally, even in the presence of excess NADPH. Curiously, in the presence of four equivalents of Trx, the enzyme does not fully reoxidize and maintains the thiolate-FAD CT. The authors therefore imply that not only does the flavin likely have a very low reduction potential but also the catalytically relevant reduced states are the EH2 and EH4.

When compiling the mechanistic and structural information for high MW TrxR, specific common attributes are made apparent. While catalyzing the same chemical reaction as low MW TrxR, these larger TrxR enzymes are more closely related to GR, TR, MR, and LipDH. The second catalytic disulfide has an elevated reduction potential and acts as a sink for electrons passing from the flavin and first catalytic disulfide. And as this moiety resides on a mobile *C*-terminal loop, it can act as a mediator transferring these electrons to the disulfide of Trx. Additionally, the flavin appears to have a very low redox potential, as the fully reduced form does not accumulate during the reductive half-reaction, even in the presence of excess NADPH. Likely the Sec found in the mammalian enzyme is present to favor the deprotonated state, though PfTrxR (which has only CysCys at the *C*-terminus) instead enhances the Cys thiol activity with the addition of a His containing loop.

3.3. Mercuric ion reductase (MerA)

Mercuric ion reductase (MerA) is a part of the mercurial detoxification system found in most eubacteria [100–102]. This cytoplasmic enzyme utilizes electrons derived from NADPH and reduce Hg^{2+} to Hg^{0} (Fig. 10A). Free Hg^{2+} is toxic as it binds to metalloproteins and is reactive with exposed cysteine residues [103]. However, the elemental form is relatively innocuous and volatile diffusing from the cell as a gas. MerA is encoded in the genes of the *mer* operon, which also includes genes for several other proteins responsible for regulation of gene expression (MerR), the uptake/transportation of mercurials (MerP and MerT), and the ligation of the *C*–Hg bonds of organomercurials (MerB) [103]. While first identified in *Escherichia coli* and *Pseudomonos aeruginosa*, Fox and Walsh were among the first to successfully purify PaMerA [100,104–106].

These researchers noted several mechanistic features that were highly reminiscent of those observed for LipDH, GR, and TrxR [100]. Given the reactivity of Hg^{2+} ions toward thiols, MerA's employment of Cys-Cys redox centers to catalyze this reduction was unexpected. Additionally, these researchers demonstrated that ~ 2 dithionite equivalents were necessary to obtain the fully reduced enzyme spectrum, indicative of at least one other redox active center in addition to the flavin. While monitoring the anaerobic titration with dithionite, these researchers noticed the accumulation and decay of an absorption feature attributed to the thiolate-FAD complex that was reported to form after the addition of ~ 1 reducing equivalent. They also quantified the presence of ~ 2 titratable thiols resolved after NADPH reduction, using DTNB assay. It was shown that 11-12 of the 16 amino acid residues of the active sites of LipDH and GR are conserved including the catalytic cysteines [26,107]. Brown et al. identified the catalytic cysteines to be at

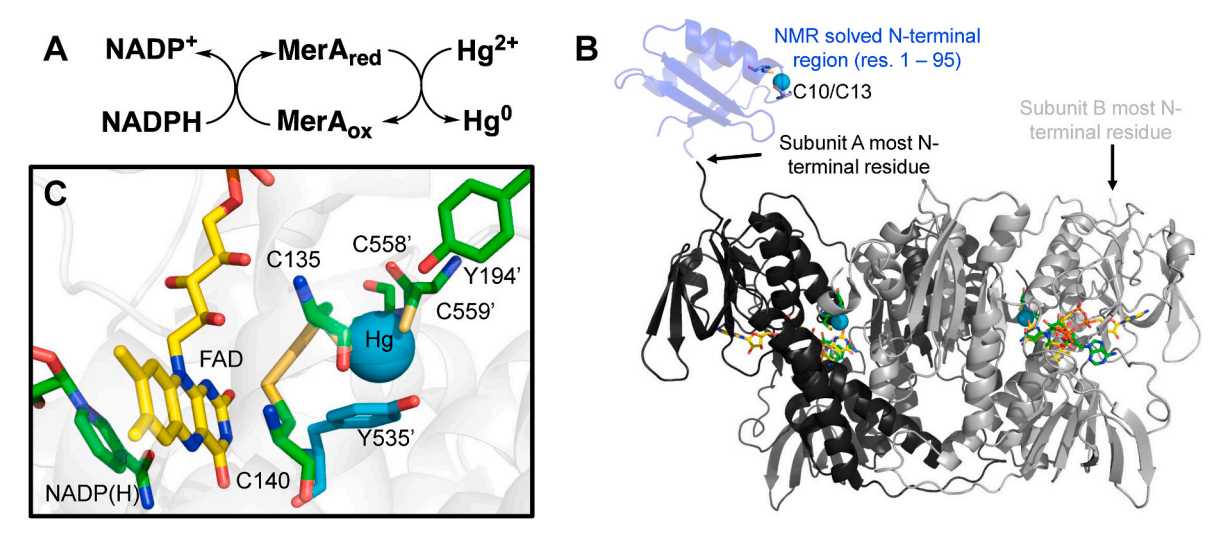


Fig. 10. MerA catalyzed reaction and overall structure. A. Overall chemical reaction catalyzed by MerA. B. Displayed in black and grey are the two subunits of the dimeric PaMerA•NADP(H)·Hg complex (PDB 4K7Z). As this structure was captured using the C135A/C140A double variant, the similar PDB structure 4K8D was overlayed to show the orientation of the Cys within the first catalytic disulfide. All published crystal structures of this enzyme were of the truncated form which lacks the *N*-terminal region including residues 2–95, However, using NMR, the secondary structure of the *N*-terminal region was solved and is shown here in blue (PDB 2KT3), with a mercury ion bound between the Cys of the proposed catalytically relevant third disulfide pair (C10/C13). As this domain's orientation within the structure is unknown, this was artificially appended to the most *N*-terminal resolved residue of Subunit A. The active site is shown in C. In all structures, the NADP(H) is shown in green, the FAD is shown in yellow, the cyan spheres indicate what the crystallographers have labeled as a Hg²⁺.

positions 135 and 140, while the analogous cysteines of HsGR and porcine LipDH are found at positions 58/63 and 45/50, respectively, suggesting that MerA contains an extended *N*-terminus [108]. While the available data was consistent with the presence of one catalytic disulfide, as structural and kinetic characterization of MerA would progress, evidence amassed for the involvement of additional catalytic disulfides.

In 1986, Miller et al. quantified the amount of exposed thiols/monomer of various PaMerA oxidized and partially reduced enzyme•ligand complexes [109]. It was demonstrated that a total of six thiols per monomer are present in the EH₂ form, while only four thiols are present in the E_{ox} state. Additionally, when Hg²⁺ is present, two of the thiols in the EH₂ state are not detectable until Hg²⁺ is displaced with the introduction of NaI. This data therefore indicated that the EH₂ state results from the reduction of one catalytic disulfide and suggested that this thiol pair is likely also responsible for binding Hg²⁺. Moreover, the introduction of Hg²⁺ to the EH₂ state did not result in the reoxidation of the enzyme prompting the proposal that the two-electron reduced state is required to bind Hg²⁺, but two additional electrons are required to reduce the metal ion [109].

The labs of Williams, Ballou, and Walsh published multiple manuscripts revealing various additional aspects of MerA's catalytic mechanism [110-113]. Unlike what was previously reported, they noted that four electrons were required when initially converting from the E_{ox} to the fully reduced state, which was readily identified by the accumulation of the thiolate-FAD CT feature [110]. It was shown that this state cannot reduce Hg^{2+} and its only when NADPH is then bound and oxidized that the Hg ion is reduced and then released. Thiol titrations and iodo-[14C]acetamide thiol labeling were used to demonstrate the C-terminal C558/C559 residues catalytic relevancy. It was suggested that these residues are in communication with the active site FAD as mutation of either Cys to Ala will perturb the flavins fluorescent qualities. Additionally, they revealed that the active site Cys pair (C135/C140) is required to reduce the C558/C559 pair. Variant enzymes were prepared with mutations made to the proximal disulfide (C135/C140) [111], all of which (including single and double mutants) appeared to be fully reduced (FADH2 state) with the introduction of just two electrons. This is consistent with electrons being transferred from the FAD to the C135/C140 thiol pair that then reduces C558/C559 pair, similar to the relay of high MW TrxR. An anaerobic analysis of the

variant enzymes' reoxidation via Hg2+-EDTA and turnover with Hg²⁺-EDTA or Hg(Cys)₂ was performed to determine if the enzyme lost the ability to transfer electrons to Hg²⁺ with the alteration of the first disulfide. These data showed that all C135 or C140 variants were unable to efficiently reduce Hg^{2+} , with most displaying a reoxidation rate similar to that of free FADH2, and all exhibiting a turnover rate 45-120 -fold slower than the wild type enzyme. Additionally, an in vivo study of several variant enzymes was performed to assess the role of the C-terminus C558/C559 pair and the third, possibly catalytic, disulfide nearer to the *N*-terminus, C10/C13 [112]. The *N*-terminal region of the enzyme was proposed to be involved in the transport of Hg²⁺ to the active site of MerA as its primary sequence was found to resemble that of the Hg²⁺ transport protein, MerP (discussed below) [114]. However, the in vivo data indicated that the C13A and C10A/C13A variants had minimal impact on cell growth. In contrast, the variant lacking the C-terminal disulfide was shown to be sensitive to HgCl2. Therefore, MerA was proposed to utilize two sets of catalytic disulfides though their individual functionality was not yet definitively known.

In the early 1990s the Pai and Walsh labs solved the first crystal structure of Bacillus sp. MerA [3,4]. This structure lacked resolution for the N-terminal domain (residues 1-166). The interpretable density included a region labeled as the core (res. 167-616) which closely resembled the structure of glutathione reductase that has the first catalytic disulfide, FAD, and NADPH binding region. As was the case with high MW TrxR, an appended C-terminus (res. 617-631) has a second catalytic disulfide within a loop that is positioned to interact with the first catalytic disulfide of the opposing subunit. The comparison of several ligand complexes revealed that, like several of the aforementioned FDR enzymes, the Bacillus MerA possess a Tyr residue at position 344 which shifts between a closed and open conformation with the binding of the NADPH. While this structure has not been deposited in the Protein Data Bank (published in the year that mandatory PDB submission came into effect), several structures of the PaMerA form of the enzyme were subsequently deposited in the early 2000s [5,115]. These crystal structures also did not resolve the N-terminal region (residues 2-95 of PaMerA). Fig. 10B depicts the dimeric structure of the PaMer-A•NADP(H)·Hg complex (PDB 4K72) [5]. This complex was captured using the C135A/C140A variant, and so a similar structure (PDB 4K8D) [5], which has these cysteines intact was overlayed to display the arrangement of the two Cys residues of the first catalytic disulfide. While all of the available structures lacked data for the N-terminal domain, the secondary structure of this domain was determined using NMR (PDB 2KT3) [6]. As this region's orientation relative to the rest of the enzyme is unknown the N-terminal segment has been artificially appended in Fig. 10B. The N-terminal region was solved with a Hg atom modeled to bridge the two Cys of the proposed third catalytic thiol pair (C10/C13). More recently, Johs et al. combined small-angled X-ray scattering and molecular dynamics simulations to model the movement of these two regions in relation to one another [116]. Their data suggests that the N-terminal region will rotate inward placing the coordinating C10/C13 residues near the core interface and C-terminal disulfide, suggesting that this additional disulfide may exist to usher Hg^{2+} to the active site. Fig. 10C displays the active site of subunit A proximal to the FAD isoalloxazine. The nicotinamide of the NADP(H) is shown to stack against the re face of the FAD isoalloxazine ring, and the first catalytic disulfide (C135/140) is positioned conventionally near the si face of the flavin. This orientation suggests that the C140 of the cystine reacts with the flavin hydroquinone during reduction. This is highly similar to the active site orientation found in LipDH, GR, TR, MR, and high MW TrxR (Figs. 3, 4 and 8). As was observed for high MW TrxR, the C-terminal C558/C559 pair is nearest to C135 of the first catalytic disulfide and is positioned to undergo disulfide/thiol exchange and/or coordinate Hg²⁺. Moreover, the structure shown has density for what is believed to be a Hg ion between the C558 and C559 thiols. Two residues Y194 and Y535' (from the opposing subunit), also coordinate to the metal ion. These residues appear to be analogous to the Y264 and Y605' of the Bacillus enzyme that were shown to coordinate to Cd²⁺ ion [3]. Collectively these residues form a roughly tetrahedral coordination sphere. In 1993, Rennex et al. characterized basic steady state kinetic properties of two single and one double variant forms of MerA in which these Tyr residues were mutated to Phe (in Bacillus sp. MerA, Y264F, Y605F, Y264 \pm 605F) [117]. The Y605F variant displayed a similar K_m and a 6-fold slower k_{cab} the Y264F had a 5-fold tighter $K_{\rm m}$ and a 160-fold slower k_{cat} , and the double variant displayed a 5-fold tighter K_m and 167-fold slower k_{cat} . These stark differences in the observed relative kinetic constants, with Hg²⁺ as the oxidant substrate, suggest that these two residues participate in metal ion acquisition as the structural data had predicted.

Additional studies were completed by the labs of Miller, Williams, Ballou, and Walsh to further characterize the enigmatic catalytic mechanism of MerA [113,118,119]. In 1990, Miller et al. trapped various reaction intermediate states with the use of the C135A/C558A/C559A triple variant, which only retains C140 [113]. With varied pH they confirmed that as the C140 residue is deprotonated the characteristic thiolate-FAD CT absorption centering around 550 nm develops. Additionally, while keeping the system at a low pH, thus maintaining the protonated state of the C140 residue, they were able to show the formation of an FAD C (4a)-Cys140 adduct with the introduction of NADP⁺. Features reminiscent of this species were reported earlier by Sahlman et al. [120]. These data revealed the direct transfer of electrons through the FAD and onto the C135/C140 pair, establishing the formation of the EH₂ complex, prior to Hg²⁺ binding.

Several years later, Engst et al. utilized transient-state approaches to attempt to assign stages of the reaction and understand the role of the C558/C559 disulfide [118]. Utilizing what was thought to be the pre-activated form of MerA, they observed the single turnover of the EH₂•NADPH complex of both the wild type and C558A/C559A enzymes. In the presence of a 10-fold excess of NADPH and a limiting concentration of HgBr₂ they observe spectral changes which they assigned to the loss of the thiolate-FAD CT as Hg²⁺ coordinates with the first thiol pair, quenching the C140 thiolate and displaying a second order rate constant of $^{\sim}8\times10^6~\text{M}^{-1}\text{s}^{-1}$. This then transitions to a quasi-steady state for which the enzyme completes several turnovers ($^{\sim}3$), with minimal spectral changes. This spectrum has long wavelength characteristics centered around 620 nm and was later confirmed to be indicative of the EH₂•NADP+•Hg²⁺ complex. As the oxidant was

limiting, reformation of the thiolate-FAD CT absorption was observed. This final spectrum additionally displays some long wavelength absorption characteristics, that were attributed to a mixture of the EH₂•NADPH and EH₂•NADP⁺ complexes. In contrast to the conclusions drawn from structural data, when performing the same experiment with the C558A/C559A variant, no significant kinetic differences were noted, suggesting that the C-terminal disulfide does not participate in the reduction of Hg²⁺. Additionally, it was shown that only when the C135 residue was also mutated (in addition to C558A/C559A) was Hg²⁺ binding diminished, confirming the requirement for both C135 and C140 residues for metal ion binding. In these experiments no significant accumulation of the reduced flavin was observed and it was proposed that after Hg²⁺ associates with the C135/C140 pair the electrons are then rapidly transferred through the FAD to reduce the Hg ion, consistent with the EH₂•NADPH complex being the active state of the enzyme. The Miller group went on to attempt to further investigate the catalytic purpose of the C-terminal disulfide [119]. Using the same spectrophotometric handles, they demonstrated that the size and affinity of the ligands coordinated to the metal ion substrate may dictate its pathway of entry into the enzymes active site. With small ligands such as HgBr₂ and Hg(CN)₂ they observe ostensibly identical MerA kinetic behavior, with or without the C-terminal disulfide. However, with bulkier ligands such as Hg(Cys)₂, Hg²⁺ binding and reduction are significantly slowed with the C558A/C559A variant. The C-terminal thiols are therefore proposed to function to displace larger ligands and aid ${\rm Hg}^{2+}$ association with the buried C135/C140 thiol pair. Upon examination of the Bacillus sp. MerA structure, these researchers also note the presence of a narrow channel leading directly to the C135/C140 pair, thought to possibly permit entry of small Hg²⁺ ions with readily dissociable ligands (HgCl₂, HgBr₂, Hg (CN)₂) and a wider channel nearer to the C558/C559 pair that may be accessed when Hg^{2+} is coordinated by the C-terminal thiols [3]. It should be noted that these conclusions were based primarily on the rate of decay of the FAD-thiolate CT absorption that by itself does not report the Hg²⁺ binding equilibrium.

More recently Lian et al. performed Quantum Mechanical/Molecular Mechanical calculations to understand the transfer of Hg^{2+} between the two Cys pairs [5]. Their model suggests that the ligand-transferring intermediate state is a tricoordinated Hg^{2+} ion which is nearly thermoneutral and more stable than the two Cys coordinated states. Their data suggests that the balance of protons and Hg^{2+} competing for the Cys thiolates creates an environment that entropically drives the sequential transfer of Hg^{2+} from the *N*-terminal Cys pair to the mobile *C*-terminal Cys pair and then to the inner most Cys pair adjacent to the flavin.

Despite its apparent structural and kinetic similarities to other one and two catalytic disulfide containing FDR enzymes (LipDH, GR/TR/ MR, and high MW TrxR), MerA would appear to utilize Cys pairs in Hg²⁺ acquisition rather than as an electron relay. Similar to disulfide/thiol exchange reactions, these Cys residues function as nucleophiles when acquiring Hg²⁺, effectively displacing coordinating ligands, but also acting as leaving groups when transferring the Hg²⁺ inward to other thiol pairs. Interestingly, while Hg²⁺ has been demonstrated to be toxic to most organisms as it tends to irreversibly coordinate to Cys residues, MerA has evolved to utilize this strong interaction while controlling the active site environment to avoid inactivation. For example, the Y605' residue of Bacillus sp. MerA is analogous to the catalytic H467' of HsGR that is shown to be required for deprotonation/activation of one of the thiols of the proximal catalytic disulfide (discussed above). With this Tyr residue, and the additionally coordinated Y264, MerA has apparently had its oxidant ligand binding sites repurposed to ensure a tri- or tetradentate coordination sphere about the metal ion. In addition, the activated state of MerA has the proximal disulfide (and possibly others) pre-reduced and NADPH is bound (EH2•NADPH complex). This allows for the rapid direct or staged association of any available Hg²⁺ ions with the proximal Cys pair, followed by the transfer of electrons through the FAD to form Hg⁰.

Over the ~40 years that this enzyme was characterized, conflicting

data as to whether the *N*-terminal disulfide is catalytically necessary has accumulated. There is minimal experimental support for the proposed movement of the *N*-terminal domain carrying the C10/C13 pair acting as a means of delivering Hg²⁺ inward. Certain groups have reported that replacing these Cys with Ala does not impact the cells survival in the presence of HgCl₂ [112], while others have reported slightly improved HgBr₂ protection with the fully intact protein when compared to just the catalytic core [115]. Early experiments demonstrate that two disulfides are likely reduced with the introduction of two equivalents of NADPH prior to reduction of the FAD. The data supports that these electrons are transferred from the FAD to the C135/C140 pair to the C558/C559 pair but no direct evidence indicates that they are then transferred to the C10/C13 disulfide.

3.4. Thioredoxin glutathione reductase (TGR)

Thioredoxin glutathione reductase (TGR) has been proposed to utilize three disulfide redox centers to catalyze the reduction of both thioredoxin (Trx) and glutathione (GSSG), harvesting electrons from NADPH. Isolation and characterization of this enzyme began in the early 2000s, with cytosolic and mitochondrial TGR being found in mature mammalian testes [121] and in several species of platyhelminths [122–126].

TGR appeared to be the primary means to maintain levels of reduced Trx and GSH in these parasitic flatworms, as these organisms seem to lack conventional TrxR and GR enzymes. They also lack catalase despite encountering high levels of oxidative incursion from the host's immune response. They therefore appear to rely exclusively on reduced forms of Trx and GSSG to recycle peroxiredoxins to ameliorate $\rm H_2O_2$ [127]. TGR has been established as a drug target to treat Platyhelminthes infections [128–132]. In mammalian testes cells, TGR has been identified to be an important regulator of the transcriptional activity of retinoic acid receptor by repairing its DNA-binding capacity after ROS damage [133] and is involved in sperm maturation [134].

With the first purifications of TGR derived from Schistosoma mansoni

(SmTGR) and mice researchers noted its similarities to other well-characterized FDR enzymes such as GR and high MW TrxR [121,122]. TGR is composed of 598–615 amino acids and a molecular weight of \sim 65 kDa, \sim 10 kDa larger than mammalian TrxR (\sim 56 kDa) or GR (\sim 55 kDa) [121]. This difference is derived from an *N*-terminal extension of \sim 100 amino acids which has a fold similar to the \sim 11 kDa thio-l/disulfide oxidoreductase, glutaredoxin (Grx). This protein is a part of the glutathione redox system and will traditionally accept electrons from GSH to catalyze reversible protein glutathionylation [135]. Of the residues 111–598 of SmTGR, \sim 64% are identical to human TrxR and \sim 36% are identical to human GR [122]. Residues 11–598 of SmTGR are \sim 55% identical to mouse TGR [122], which in turn shares \sim 88% sequence identity with human TGR [121].

The crystal structure of SmTGR was first solved in 2008 [136]. This 2.2 Å structure (PDB 2V6O) was derived from an expression construct that lacked sequence for the last two residues including one of the residues of the catalytically relevant selenide-sulfide, Sec597, and Gly598. As predicted the structure was revealed to be a fusion of a Grx domain (res. 1-106) and a catalytic core TrxR/GR domain (res. 107-598). This core region was highly similar to mammalian TrxR, possessing an NADPH and FAD binding region, one disulfide pair stacked against the flavin, and a C-terminal extended loop. The presence of four conserved potentially catalytic disulfide (or selenide-sulfide) pairs was indicated. These were the C154/C159 pair which is positioned directly adjacent to the FAD, the C596/U597 pair that is located before the final residue of the C-terminus (Gly598), and the C28/C31 pair of the Grx domain. An additional disulfide pair is formed by SmTGR C520/C574 residues and exists nearer to the dimer interface. In this structure however, this disulfide is reduced, and the cysteine thiols 6.1 Å distant.

Two years later, Angelucci et al. published the crystal structure of the full-length enzyme and enzyme•ligand complexes [11]. Fig. 11 depicts the partially reduced SmTGR structure with one resolved C-terminus (PDB 2 \times 8C) extending into the active site of the opposing subunit [11]. The inset of Fig. 11 includes the overlaid structure of the PtGrx (PDB 1Z7R) with the 106 N-terminal residues of SmTGR. Though the

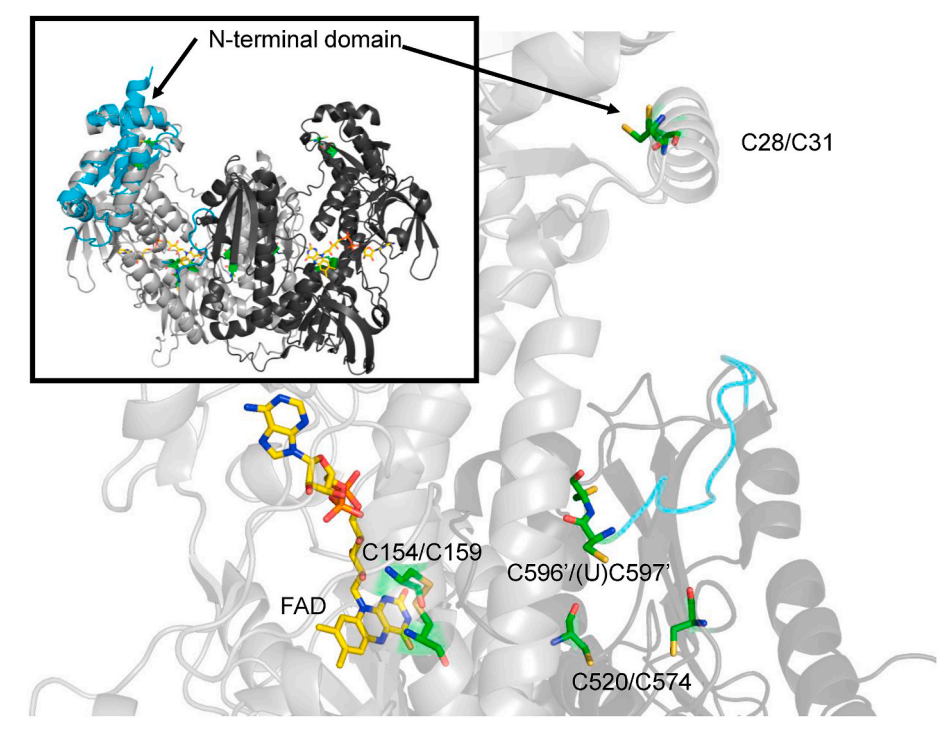


Fig. 11. The Structure of TGR. The overall dimeric structures of SmTGR (PDB $2 \times 8C$) is shown in Inset. The SmTGR dimer in which the *N*-terminal appended domain is shown aligned with the glutaredoxin from aspen (PDB ID 1Z7R). Main Figure. The proposed electron relay of SmTGR of subunit A. The C596/(U)C597 residues are from subunit B and reside on a loop shown in cyan.

SmTGR \bullet SmTrx complex has not been captured crystallographically, when comparing TGR's structure to Fig. 9 one can surmise that the association of Trx and the conformational change of the mobile C-terminus is likely similar to that observed with high MW TrxR. Additionally, in the crystalized SmTGR \bullet GSH complex (PDB 2 \times 8H) (not shown), the GSH product is bound near the C28/C31 disulfide [11]. Using computational modeling, the C-terminal loop was proposed to shift conformation with the terminal selenide-sulfide acting as shuttle between C154/C159, Trx and C28/C31 [11]. Also annotated in Fig. 11 is the C520/C574 pair that has not been shown to be catalytically relevant. While the parasitic form of TGR has been crystallized several times there is no deposited structure of mammalian TGR, however due to their sequence similarity both forms likely have similar electron relays.

In addition to the above structural information, more recently several researchers have identified an apparent regulatory residue adjacent to the nicotinamide binding site [137]. As was the case with GR, TR, high MW TrxR, and *Bacillus* sp. MerA, the displacement of the side chain of a conserved Tyr (Y296 of SmTGR) residue away from the flavin coincided with NADPH association (discussed above). The precise role of these highly conserved aromatic residues has not been well understood. However, the functionality of the Y296 of SmTGR was investigated and may demonstrate the catalytic role of positionally equivalent residues in the FDR enzyme family (discussed below). The residues adjacent to Y296 that form what has been coined as the "doorstop" pocket are unique in each enzyme in which they occur [137] and these differences have led researchers to pursue selective inhibitors of the parasitic form of TGR [138,139].

Characterization of both mammalian and platyhelminth forms TGR has been attempted. SmTGR has been proposed to catalyze the reversible reduction of GSSG, Trx, and glutathionylated peptides. However, much of these studies were completed under aerobic conditions monitoring the steady state turnover of TGR with various disulfide containing [121,122,140–144]. To quantify the Michaelis-Menten constants, researchers either tracked NADPH oxidation (which in the presence of oxygen would be artificially elevated [145]), would monitor the reaction of TGR with DTNB (which will readily react with any exposed thiol, but is not a native substrate of the enzyme), or they would complete a coupled reaction for which the reporter would be the measurement of the rate of insulin precipitation at 650 nm, after it was reduced by Trx [146]. Each of these tracking methods included complications that made definitive observations of the catalytic function of TGR difficult to obtain.

Several researchers also performed anaerobic titrations to characterize the reductive and oxidative half-reactions of TGR. Angelucci et al. over-reduced the "truncated" enzyme, which was lacking the last two amino acid residues, by introducing four equivalents of NADPH and subsequent flavin reoxidation in the presence excess GSSG [136]. The reduced enzyme displayed absorption characteristics reminiscent of flavin reduction and thiolate-FAD CT, revealing the accumulation of intermediate reduced state(s) and demonstrating its similarity to other FDR enzymes. Huang et al. also completed a titrative anaerobic reductive half-reaction of the U597C variant of SmTGR [142] where they titrated equivalents of NADPH/mol of FAD and monitored the spectrophotometric changes. Flavin reduction appeared to coincide with the development of the thiolate-FAD CT absorption and the enzyme appeared to reach a maximally reduced redox equilibrium (at which the extent of flavin reduction and thiolate-FAD CT formation is unchanging) with the introduction of 4-fold NADPH. Accordingly, the authors concluded that TGR possess three redox moieties in addition to the flavin. Interestingly, in this state the overall extent of flavin reduction is minimal, though difficult to quantify as the thiolate-FAD CT contributes maximally at 450 nm [147].

As most of the FDR enzymes described accumulate multiple intermediate states during the reductive and oxidative half-reactions, many have been studied using transient state methods to discern the pathway of electron transport. Along with the previously mentioned data, Angelucci et al. also performed a minimal transient state analysis of SmTGR's reductive and oxidative half-reactions; however, this data is limited and has a low signal to noise ratio as a result of the enzyme concentrations used [11]. Several years later, the Moran lab attempted to characterize the mechanism of SmTGR utilizing anaerobic transient state techniques with the WT and several variant enzymes [145,147]. These researchers monitored and assigned various intermediate states to describe the overall sequence of electron transfer. As SmTGR was expressed heterologously in E. coli cells, these researchers mutated the U597 residue to a Cys to avoid incomplete Sec incorporation, and allow for high yielding, homogeneous enzyme preparation. In the presence of oxygen they reported an apparent ~2.5-fold increase and ~4-fold increase in the turnover of SmTGR with SmTrx and GSSG, respectively [145], demonstrating the requirement for anaerobiosis for valid kinetic observations. Utilizing limiting NADPH concentrations, these researchers evaluated the enzyme's reductive half-reaction by monitoring the absorption of the flavin and associated complexes. The kinetic traces obtained delineate into five phases. With introduction of NADPH, rapid flavin reduction concomitant with the formation of a charge transfer absorption centered at 650 nm is observed. This CT is assigned to the formation of the NADP⁺-FADH₂ complex as its full accumulation occurs with significant NADPH oxidation and FAD reduction. Though NADPH is limiting in all reactions, the researchers report relative low accumulation of reduced flavin (\sim 35%). The researchers suggest this is a result of the near equal rate of flavin reduction and reoxidation that occurs with reduction of the proximal disulfide (C154/C159), thus indicating that the flavin has a lower reduction potential than NADPH and other redox centers in the electron relay. Electrons acquired at the flavin were shown to be transferred to the first catalytic disulfide (C154/C159) by accumulation of a thiolate-FAD CT absorption feature. The extent of accumulation of this feature was diminished at high concentrations of $\mathrm{NADP}^+,$ which the authors suggest indicates that NADP^+ must dissociate from the enzyme prior to the deprotonation of the thiol. This is then followed by two flavin reoxidation events which the authors assigned to the electrons flowing further into the enzyme. Both events are delineated from one another, and the staged or stepped nature of the flavin reoxidation is most apparent at NADPH concentrations nearly equimolar with the enzyme. While this staged flavin oxidation is indicative of more complexity the authors acknowledge that these observations do not allow for the direct assignment of each of these events, however they proposed that this may reflect the movement of electrons onto the C596/C597 pair and subsequently onto the C28/C31 pair of the Grx domain. Interestingly, even with limiting NADPH available the enzyme does not fully reoxidize, although all CT signals are lost when the system comes to equilibrium. This suggests that electrons are likely shared among all the redox centers in the absence of oxidant substrates. When introducing GSSG the kinetics of the reductive half-reaction of SmTGR does not appear to change, even at oxidant concentrations ~10-fold that of the enzyme concentration. This, with the demonstration that the observed anaerobic rate of turnover with GSSG was significantly slower than any process observed in the transient-state analysis, suggests that GSSG binding/reduction is not part of the transient state data. When titrating SmTrx the two flavin oxidation phases blend into one event which approached the rate of anaerobic turnover with Trx as the oxidating substrate. It was proposed that in the presence of Trx, electrons do not accumulate on the C596/C597 pair and instead transfer to the Trx disulfide. In addition, the reductive half-reaction with Pro-S deuterated NADPD confirmed that this is the hydride transferred to reduce FAD and that the same hydride is also transferred to reduce the first disulfide pair, and becomes the proton removed to generate the thiolate-FAD CT.

This same group continued to explore the catalytic mechanism of TGR utilizing several variant enzymes to trap intermediate states in an attempt to solidify the pathway of electron transfer [147]. The variants studied include point mutations made to one of the Cys of each of the proposed catalytic pairs (C159S, U597S, and C31S) and the mutation of H571′ and Y296 residues to alanine. For the C159S variant, the phase of

the reductive half reaction that results in flavin reduction and long wavelength CT formation was slowed and separated into two events, of which only the rate constant for the first phase titrated with increasing NADPH concentration and was fit to determine an approximate K_{NADPH} \sim 7 μ M. The deconvoluted spectra revealed the formation of an additional CT (centered at 600 nm) which was assigned to the stacking of NADPH-FAD. This was then followed by minimal flavin reduction and formation of the NADP⁺-FADH₂ CT (centered at 680 nm). Importantly, the reductive half-reaction of the C159S variant revealed no thiolate-FAD CT signal, confirming that the C159 thiolate is the origin of this signal. The C159S variant effectively traps the electrons at the flavin and when mixed with excess NADPH in deuterated buffer the researchers monitored the rapid exchange of the Pro-S hydride for solvent deuteride using NMR spectroscopy. This indicated that the reduction of the flavin by NADPH is reversible, suggesting that the redox potential of NADPH and SmTGR's FAD are similar. Conversely, in the reductive half-reaction of the U597S variant the thiolate-FAD CT absorption forms and is sustained. This is consistent with the notion that the C-terminal selenide-sulfide pair (C596/U597) is the relay sequence and when this pair is nullified by mutation the enzyme cannot readily reoxidize. When introducing excess SmTrx oxidant in the presence of limiting NADPH, the observed kinetics of this variant are unchanging relative to the C596/U597C WT facsimile enzyme, indicating that the C596/U597 residues are necessary to transfer electrons to thioredoxin. The reductive half-reaction of the C31S variant is nearly identical to that of the U597C enzyme consistent with the reduction of the distal C28/C31 disulfide not registering in the reductive half-reaction. This data therefore indicates that the observed flavin reoxidation and subsequent loss of the thiolate-FAD CT signal is related to the transfer of electrons to the C-terminal selenide-sulfide. However, the reason for the delineation of this process into two phases is unclear. It was proposed that these two events demonstrate various conformational changes associated with the mobile C-terminal loop that kinetically yields staged flavin reoxidation/loss of thiolate-FAD CT. This was interpreted as electrons penetrating further into the enzymes redox centers while maintaining quasi equilibrium redox exchange with the flavin. The first of which is tentatively assigned to the movement required to transfer electrons to the C34/C37 disulfide of SmTrx, while the second, which is kinetically or thermodynamically hindered by comparison may be attributable to the C-terminal conformational change required to orient the C596/U597 pair proximal to the C28/C31 disulfide.

The Y297 residue had previously been shown crystallographicaly to change conformations with the binding of the NADPH apparently modulating access to the isoalloxazine N5. The Y297A variant has a ~30-45-fold slower rate of flavin reduction compared to the U597C variant. When either enzyme is reacted with excess dithionite, the flavin of the Y296A variant reduces ~ 175 -fold faster than that of the U597C variant indicating that the Y296 residue likely functions both to prevent non-specific reduction of the flavin while also influencing the acquisition of NADPH and the hydride transfer reaction. Analogous to H467'of HsGR, H571' of SmTGR interacts with the first catalytic disulfide of the opposing subunit and is thought to act as a catalytic base to deprotonate either thiol (Fig. 4). When monitoring 540 nm with the H571A variant two phases are revealed prior to the formation of the thiolate-FAD CT. These events are proposed to be the accumulation of the NADPH-FAD CT (now unveiled at 540 nm as the thiolate-FAD CT absorption is no longer overlapping) followed by the decay of this feature with the reduction of the C154/C159 disulfide, prior to the C159 thiol deprotonation. The thiolate-FAD CT absorption accumulates but at a rate ~17-fold slower than when H571 is present.

Together, crystal structures and transient state analyses confirm the sequential order of electron transfer to be from the Pro-S hydride of NADPH to the FAD, and then to C154/C159 disulfide, and then on to the C596/U597 pair. While these phases can tentatively be assigned to the movement of electrons away from the flavin, likely as the *C*-terminal loop shifts conformation, the involvement of the C28/C31 disulfide was

not confirmed from these data [147]. Aside from the observed complex of a GSH molecule proximal to this disulfide pair in the SmTGR•GSH complex crystal structure (PDB 2 × 8H) [11] and the observation that 4 reducing equivalents are needed for maximal flavin reduction/thiolate formation [142], there is minimal evidence of the involvement of the putative Grx domain and the observed anaerobic steady state turnover number with GSSG as the oxidant is significantly slower than events observed under transient state conditions [145].

4. Conclusion

While the FDR enzymes discussed within this review vary in both complexity and chemistry catalyzed, all have core conserved catalytic machinery that initiates an electron relay within enzyme. While the electron pathway is tailored to specific purposes, most FDR enzymes have evolved to utilize similar neighboring residues for regulation, substrate binding, and to enhance reactivity. Fig. 12 depicts the general overall catalytic sequences of the FDR enzymes. While it does not include all the complexities of each enzyme, it serves as a visual reference for the core activities of this family of enzymes. Although absent in the LipDH, low MW TrxR, and AhpF catalytic mechanisms, several FDR enzymes possess a conserved Tyr (or Phe) residue within the NAD(P)H binding pocket that is observed to change conformation with the association of this co-substrate. This residue functions to regulate the binding of the nicotinamide while also blocking the flavin isoalloxazine N5 from interaction with other reductant molecules, thereby acting as a gating residue. LipDH functions physiologically in the reverse direction, accepting electrons from dihydrolipoamide and reducing NAD⁺, and therefore does not require this regulatory residue. Additionally, both low MW TrxR and AhpF have been shown to possess alternative conformations for regulatory control of the binding of NAD(P)H, though the precise catalytic relevancy of each conformation is not well understood.

Some FDR enzymes are observed to possess a conserved His residue which functions as a catalytic base to deprotonate one of the Cys of the first disulfide pair. While this function has been proposed in several previous studies, the more recent characterization of the SmTGR H571A variant cleanly demonstrates that this residue exists to increase the reactivity of the nascent thiol pair nearest to the flavin and induces the characteristic FAD-thiolate charge transfer absorption. Due to their structural dissimilarity to other enzymes within this subclass, a corresponding residue has not definitively been identified for both low MW TrxR and AhpF. Opposingly, within MerA a Tyr residue is found in an analogous position to this His residue and is proposed instead to stabilize the reactivity of the Hg²⁺ ion when coordinated to the first Cys/Cys pair.

While LipDH, GR, TR, MR, and low MW TrxR only utilize one catalytic disulfide pair, AhpF, MerA, high MW TrxR and TGR incorporate the use of a third (and sometimes fourth) redox moiety. Therefore, while most of the less complex enzymes do complete one intermolecular disulfide exchange to reduce their substrate, the others are thought to catalyze several intramolecular disulfide (or selenide-sulfide) exchanges (Fig. 12). In the case of AhpF this second pair is found within a fused Trxlike region, while for all others it is observed at the end of dynamic Cterminus. In most crystal structures this terminus is unresolved, however in those that it was captured it can be observed to interact with the active site of the opposing subunit of the homodimer. The mobility of this loop has been theorized to be necessary to physically relocate electrons out of the active site (or for MerA to move a Hg²⁺ ion inward). The incorporation of a Sec within the C-terminal selenide-sulfide pair (2nd pair in relay) of some forms of TGR and high MW TrxR is likely negating the need for an adjacent His (or other catalytic base) as this residue has a lower pKa (~5) and therefore remains ionized at physiological pHs. Conversely, within the Plasmodium falciparum form of TrxR two Cys are found at the C-terminus but an additional loop containing a catalytic His has been identified to stack adjacent (Fig. 9), thus increasing the Cys reactivity.

Though currently poorly understood, the involvement of the N-

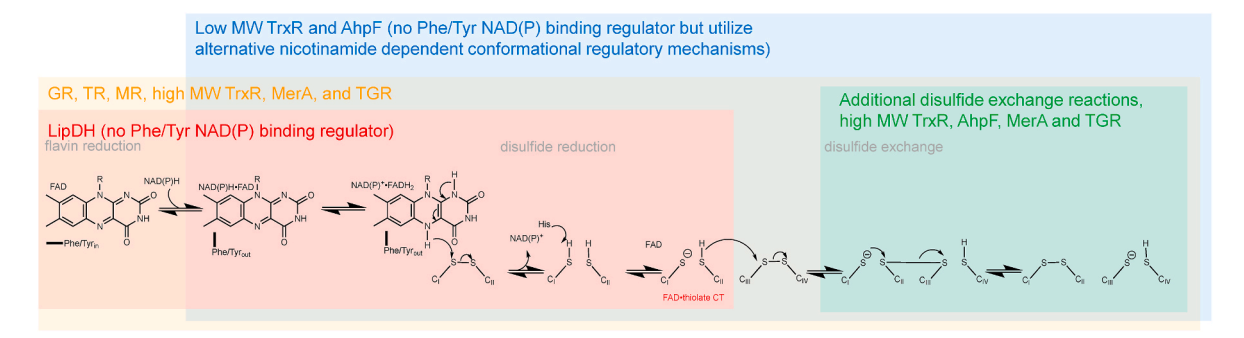


Fig. 12. Summative Catalytic Mechanism Utilized by FDRs. Here the overall catalytic mechanism of the subclass of FDR enzymes mentioned within this review has been encompassed. Though some exceptions do exist, each of the nine enzymes discussed utilize fundamentally the same chemical reactions. While a catalytically relevant His residue was identified in most of the FDRs, due to structural differences in the case of low MW TrxR and AhpF, as well as altered Cys reactivity in MerA, these enzymes do not appear to possess a catalytic base adjacent to their redox centers. Additionally, the blue and red boxes indicate that LipDH, low MW TrxR, and AhpF are not oberserved to have a conformationally active Tyr (or Phe) residue within the nicotinamide binding site, though low MW TrxR and AhpF have been shown to utilize an alternative NAD(P)H dependent domain conformational shift. The green box is indicative of the FDR enzymes proposed to utilize more than one catalytic disulfide (or selenide-sulfide) pair, though as all enzymes are demonstrated to either accept electrons from or reduce a disulfide containing substrate all enzymes will complete at least on disulfide exchange reaction.

terminal extended regions of both MerA and TGR have been suggested to provide an additional catalytic disulfide. In the case of MerA this region was proposed to be involved in the shuttling of Hg²⁺ ions from solution into contact with the *C*-terminal pair. Within TGR this *N*-terminal region has been shown to be structurally similar to glutaredoxin and has been observed to bind GSH in the TGR•GSH complex crystal structure. Whether utilizing one extra disulfide pair (in the case of AhpF and high MW TrxR) or possibly multiple (in MerA and TGR) these enzymes would appear to employ a system of connecting substrate-like protein domains to act as another electron acceptor, either to provide accessibility to bulky substrates and/or to displace electrons from the flavin. MerA would appear to be the most unusual as rather than using its chain of disulfides to transfer electrons, it instead appears to use these to both stabilize and transfer Hg^{2+} ions to the active site. Therefore, though their mechanisms may not be identical, each of these enzymes has adapted a system which either promotes or stabilizes reactivity based on the catalytic needs. The noticeable consistencies observed when comparing the structures and mechanisms of these enzymes not only allows for a more complete understanding of each enzyme independently but serves as a foundation for understanding uncharacterized FDR enzymes.

CRediT authorship contribution statement

Madison M. Smith: Writing – review & editing, Writing – original draft. **Graham R. Moran:** Writing – review & editing.

References

- A. Argyrou, J.S. Blanchard, Flavoprotein disulfide reductases: advances in chemistry and function, Prog. Nucleic Acid Res. Mol. Biol. 78 (2004) 89–142.
- [2] C.H. Williams, L.D. Arscott, S. Muller, B.W. Lennon, M.L. Ludwig, P.F. Wang, D. M. Veine, K. Becker, R.H. Schirmer, Thioredoxin reductase two modes of catalysis have evolved, Eur. J. Biochem. 267 (20) (2000) 6110–6117.
- [3] N. Schiering, W. Kabsch, M.J. Moore, M.D. Distefano, C.T. Walsh, E.F. Pai, Structure of the detoxification catalyst mercuric ion reductase from Bacillus sp. strain RC607, Nature 352 (6331) (1991) 168–172.
- [4] M.J. Moore, M.D. Distefano, C.T. Walsh, N. Schiering, E.F. Pai, Purification, crystallization, and preliminary x-ray diffraction studies of the flavoenzyme mercuric ion reductase from Bacillus sp. strain RC607, J. Biol. Chem. 264 (24) (1989) 14386–14388.
- [5] P. Lian, H.B. Guo, D. Riccardi, A. Dong, J.M. Parks, Q. Xu, E.F. Pai, S.M. Miller, D. Q. Wei, J.C. Smith, H. Guo, X-ray structure of a Hg2+ complex of mercuric reductase (MerA) and quantum mechanical/molecular mechanical study of Hg2+ transfer between the C-terminal and buried catalytic site cysteine pairs, Biochemistry 53 (46) (2014) 7211–7222.
- [6] R. Ledwidge, B. Hong, V. Dotsch, S.M. Miller, NmerA of Tn501 mercuric ion reductase: structural modulation of the pKa values of the metal binding cysteine thiols, Biochemistry 49 (41) (2010) 8988–8998.

- [7] E.F. Pai, G.E. Schulz, The catalytic mechanism of glutathione reductase as derived from x-ray diffraction analyses of reaction intermediates, J. Biol. Chem. 258 (3) (1983) 1752–1757.
- [8] H.F. Gilbert, Molecular and cellular aspects of thiol-disulfide exchange, Adv. Enzymol. Relat. Area Mol. Biol. 63 (1990) 69–172.
- [9] A. Vlamis-Gardikas, The multiple functions of the thiol-based electron flow pathways of Escherichia coli: eternal concepts revisited, Biochim. Biophys. Acta 1780 (11) (2008) 1170–1200.
- [10] H. Bauer, V. Massey, L.D. Arscott, R.H. Schirmer, D.P. Ballou, C.H. Williams Jr., The mechanism of high Mr thioredoxin reductase from Drosophila melanogaster, J. Biol. Chem. 278 (35) (2003) 33020–33028.
- [11] F. Angelucci, D. Dimastrogiovanni, G. Boumis, M. Brunori, A.E. Miele, F. Saccoccia, A. Bellelli, Mapping the catalytic cycle of Schistosoma mansoni thioredoxin glutathione reductase by X-ray crystallography, J. Biol. Chem. 285 (42) (2010) 32557–32567.
- [12] D.S. Berkholz, H.R. Faber, S.N. Savvides, P.A. Karplus, Catalytic cycle of human glutathione reductase near 1 A resolution, J. Mol. Biol. 382 (2) (2008) 371–384.
- [13] R.E. Huber, R.S. Criddle, Reprint of: comparison of the chemical properties of selenocysteine and selenocystine with their sulfur analogs, Arch. Biochem. Biophys. 726 (2022) 109233.
- [14] C.H. Williams Jr., G. Zanetti, L.D. Arscott, J.K. McAllister, Lipoamide dehydrogenase, glutathione reductase, thioredoxin reductase, and thioredoxin, J. Biol. Chem. 242 (22) (1967) 5226–5231.
- [15] N.R. Glasser, B.X. Wang, J.A. Hoy, D.K. Newman, The pyruvate and alphaketoglutarate dehydrogenase complexes of Pseudomonas aeruginosa catalyze pyocyanin and phenazine-1-carboxylic acid reduction via the subunit dihydrolipoamide dehydrogenase, J. Biol. Chem. 292 (13) (2017) 5593–5607.
- [16] V. Massey, Q.H. Gibson, C. Veeger, Intermediates in the catalytic action of lipoyl dehydrogenase (diaphorase), Biochem. J. 77 (2) (1960) 341–351.
- [17] A.J. Schierbeek, M.B. Swarte, B.W. Dijkstra, G. Vriend, R.J. Read, W.G. Hol, J. Drenth, C. Betzel, X-ray structure of lipoamide dehydrogenase from Azotobacter vinelandii determined by a combination of molecular and isomorphous replacement techniques, J. Mol. Biol. 206 (2) (1989) 365–379.
- [18] A. Mattevi, G. Obmolova, J.R. Sokatch, C. Betzel, W.G. Hol, The refined crystal structure of Pseudomonas putida lipoamide dehydrogenase complexed with NAD + at 2.45 A resolution, Proteins 13 (4) (1992) 336–351.
- [19] A. Argyrou, J.S. Blanchard, B.A. Palfey, The lipoamide dehydrogenase from Mycobacterium tuberculosis permits the direct observation of flavin intermediates in catalysis, Biochemistry 41 (49) (2002) 14580–14590.
- [20] A. Mattevi, A.J. Schierbeek, W.G. Hol, Refined crystal structure of lipoamide dehydrogenase from Azotobacter vinelandii at 2.2 A resolution. A comparison with the structure of glutathione reductase, J. Mol. Biol. 220 (4) (1991) 975–994.
- [21] R. Bryk, N. Arango, C. Maksymiuk, A. Balakrishnan, Y.T. Wu, C.H. Wong, T. Masquelin, P. Hipskind, C.D. Lima, C. Nathan, Lipoamide channel-binding sulfonamides selectively inhibit mycobacterial lipoamide dehydrogenase, Biochemistry 52 (51) (2013) 9375–9384.
- [22] J. Benen, W. van Berkel, Z. Zak, T. Visser, C. Veeger, A. de Kok, Lipoamide dehydrogenase from Azotobacter vinelandii: site-directed mutagenesis of the His450-Glu455 diad. Spectral properties of wild type and mutated enzymes, Eur. J. Biochem. 202 (3) (1991) 863–872.
- [23] J. Benen, W. van Berkel, N. Dieteren, D. Arscott, C. Williams Jr., C. Veeger, A. de Kok, Lipoamide dehydrogenase from Azotobacter vinelandii: site-directed mutagenesis of the His450-Glu455 diad. Kinetics of wild-type and mutated enzymes, Eur. J. Biochem. 207 (2) (1992) 487–497.
- [24] A.H. Westphal, A. Fabisz-Kijowska, H. Kester, P.P. Obels, A. de Kok, The interaction between lipoamide dehydrogenase and the peripheral-componentbinding domain from the Azotobacter vinelandii pyruvate dehydrogenase complex, Eur. J. Biochem. 234 (3) (1995) 861–870.

- [25] A. Argyrou, G. Sun, B.A. Palfey, J.S. Blanchard, Catalysis of diaphorase reactions by Mycobacterium tuberculosis lipoamide dehydrogenase occurs at the EH4 level, Biochemistry 42 (7) (2003) 2218–2228.
- [26] C. Thorpe, C.H. Williams Jr., Lipoamide dehydrogenase from pig heart. Pyridine nucleotide induced changes in monoalkylated two-electron reduced enzyme, Biochemistry 20 (6) (1981) 1507–1513.
- [27] N. Hopkins, C.H. Williams Jr., Characterization of lipoamide dehydrogenase from Escherichia coli lacking the redox active disulfide: C44S and C49S, Biochemistry 34 (37) (1995) 11757–11765.
- [28] L. Sahlman, C.H. Williams Jr., Titration studies on the active sites of pig heart lipoamide dehydrogenase and yeast glutathione reductase as monitored by the charge transfer absorbance, J. Biol. Chem. 264 (14) (1989) 8033–8038.
- [29] K. Maeda-Yorita, G.C. Russell, J.R. Guest, V. Massey, C.H. Williams Jr., Modulation of the oxidation-reduction potential of the flavin in lipoamide dehydrogenase from Escherichia coli by alteration of a nearby charged residue, K53R, Biochemistry 33 (20) (1994) 6213–6220.
- [30] K. Maeda-Yorita, G.C. Russell, J.R. Guest, V. Massey, C.H. Williams Jr., Properties of lipoamide dehydrogenase altered by site-directed mutagenesis at a key residue (1184Y) in the pyridine nucleotide binding domain, Biochemistry 30 (51) (1991) 11788-11705
- [31] G.L. Newton, K. Arnold, M.S. Price, C. Sherrill, S.B. Delcardayre, Y. Aharonowitz, G. Cohen, J. Davies, R.C. Fahey, C. Davis, Distribution of thiols in microorganisms: mycothiol is a major thiol in most actinomycetes, J. Bacteriol. 178 (7) (1996) 1990–1995.
- [32] T. Battista, G. Colotti, A. Ilari, A. Fiorillo, Targeting trypanothione reductase, a key enzyme in the redox trypanosomatid metabolism, to develop new drugs against leishmaniasis and trypanosomiases, Molecules 25 (8) (2020).
- [33] J. Kuriyan, X.P. Kong, T.S. Krishna, R.M. Sweet, N.J. Murgolo, H. Field, A. Cerami, G.B. Henderson, X-ray structure of trypanothione reductase from Crithidia fasciculata at 2.4-A resolution, Proc. Natl. Acad. Sci. U. S. A. 88 (19) (1991) 8764–8768.
- [34] P.A. Karplus, G.E. Schulz, Refined structure of glutathione reductase at 1.54 A resolution, J. Mol. Biol. 195 (3) (1987) 701–729.
- [35] V.S. Stoll, S.J. Simpson, R.L. Krauth-Siegel, C.T. Walsh, E.F. Pai, Glutathione reductase turned into trypanothione reductase: structural analysis of an engineered change in substrate specificity, Biochemistry 36 (21) (1997) 6437–6447.
- [36] C.S. Bond, Y. Zhang, M. Berriman, M.L. Cunningham, A.H. Fairlamb, W. N. Hunter, Crystal structure of Trypanosoma cruzi trypanothione reductase in complex with trypanothione, and the structure-based discovery of new natural product inhibitors, Structure 7 (1) (1999) 81-89.
- [37] E.M. Jacoby, I. Schlichting, C.B. Lantwin, W. Kabsch, R.L. Krauth-Siegel, Crystal structure of the Trypanosoma cruzi trypanothione reductase, Mepacrine Complex, Proteins 24 (1) (1996) 73–80.
- [38] P. Baiocco, G. Poce, S. Alfonso, M. Cocozza, G.C. Porretta, G. Colotti, M. Biava, F. Moraca, M. Botta, V. Yardley, A. Fiorillo, A. Lantella, F. Malatesta, A. Ilari, Inhibition of Leishmania infantum trypanothione reductase by azole-based compounds: a comparative analysis with its physiological substrate by X-ray crystallography, ChemMedChem 8 (7) (2013) 1175–1183.
- [39] L. Salmon-Chemin, E. Buisine, V. Yardley, S. Kohler, M.A. Debreu, V. Landry, C. Sergheraert, S.L. Croft, R.L. Krauth-Siegel, E. Davioud-Charvet, 2- and 3-substituted 1,4-naphthoquinone derivatives as subversive substrates of trypanothione reductase and lipoamide dehydrogenase from Trypanosoma cruzi: synthesis and correlation between redox cycling activities and in vitro cytotoxicity, J. Med. Chem. 44 (4) (2001) 548–565.
- [40] A. Kumar, W. Nartey, J. Shin, M.S.S. Manimekalai, G. Gruber, Structural and mechanistic insights into mycothiol disulphide reductase and the mycoredoxin-1alkylhydroperoxide reductase E assembly of Mycobacterium tuberculosis, Biochim. Biophys. Acta Gen. Subj. 1861 (9) (2017) 2354–2366.
- [41] R.L. Krauth-Siegel, L.D. Arscott, A. Schonleben-Janas, R.H. Schirmer, C. H. Williams Jr., Role of active site tyrosine residues in catalysis by human glutathione reductase, Biochemistry 37 (40) (1998) 13968–13977.
- [42] P. Rietveld, L.D. Arscott, A. Berry, N.S. Scrutton, M.P. Deonarain, R.N. Perham, C. H. Williams Jr., Reductive and oxidative half-reactions of glutathione reductase from Escherichia coli, Biochemistry 33 (46) (1994) 13888–13895.
- [43] A. Borges, M.L. Cunningham, J. Tovar, A.H. Fairlamb, Site-directed mutagenesis of the redox-active cysteines of Trypanosoma cruzi trypanothione reductase, Eur. J. Biochem. 228 (3) (1995) 745–752.
- [44] C.C. Bohme, L.D. Arscott, K. Becker, R.H. Schirmer, C.H. Williams Jr., Kinetic characterization of glutathione reductase from the malarial parasite Plasmodium falciparum. Comparison with the human enzyme, J. Biol. Chem. 275 (48) (2000) 37317–37323
- [45] M.P. Patel, J.S. Blanchard, Mycobacterium tuberculosis mycothione reductase: pH dependence of the kinetic parameters and kinetic isotope effects, Biochemistry 40 (17) (2001) 5119–5126.
- [46] M.P. Patel, J.S. Blanchard, Expression, purification, and characterization of Mycobacterium tuberculosis mycothione reductase, Biochemistry 38 (36) (1999) 11827–11833.
- [47] L.D. Arscott, C. Thorpe, C.H. Williams Jr., Glutathione reductase from yeast. Differential reactivity of the nascent thiols in two-electron reduced enzyme and properties of a monoalkylated derivative, Biochemistry 20 (6) (1981) 1513–1520.
- [48] L.D. Arscott, D.M. Veine, C.H. Williams Jr., Mixed disulfide with glutathione as an intermediate in the reaction catalyzed by glutathione reductase from yeast and as a major form of the enzyme in the cell, Biochemistry 39 (16) (2000) 4711–4721.
- [49] J. Lu, A. Holmgren, The thioredoxin antioxidant system, Free Radic. Biol. Med. 66 (2014) 75–87.

- [50] J. Kuriyan, T.S. Krishna, L. Wong, B. Guenther, A. Pahler, C.H. Williams Jr., P. Model, Convergent evolution of similar function in two structurally divergent enzymes, Nature 352 (6331) (1991) 172–174.
- [51] C.H. Williams, Mechanism and structure of thioredoxin reductase from Escherichia coli, Flavoprotein Struc. Mech. 6 (1995) 1267–1276.
- [52] G. Waksman, T.S. Krishna, C.H. Williams Jr., J. Kuriyan, Crystal structure of Escherichia coli thioredoxin reductase refined at 2 A resolution. Implications for a large conformational change during catalysis, J. Mol. Biol. 236 (3) (1994) 800-816
- [53] S.B. Mulrooney, C.H. Williams Jr., Evidence for two conformational states of thioredoxin reductase from Escherichia coli: use of intrinsic and extrinsic quenchers of flavin fluorescence as probes to observe domain rotation, Protein Sci. 6 (10) (1997) 2188–2195.
- [54] B.W. Lennon, C.H. Williams Jr., M.L. Ludwig, Twists in catalysis: alternating conformations of Escherichia coli thioredoxin reductase, Science 289 (5482) (2000) 1190–1194.
- [55] B.W. Lennon, C.H. Williams Jr., M.L. Ludwig, Crystal structure of reduced thioredoxin reductase from Escherichia coli: structural flexibility in the isoalloxazine ring of the flavin adenine dinucleotide cofactor, Protein Sci. 8 (11) (1999) 2366–2379.
- [56] E.C. Moore, P. Reichard, L. Thelander, Enzymatic synthesis of deoxyribonucleotides.V. Purification and properties of thioredoxin reductase from Escherichia coli B, J. Biol. Chem. 239 (1964) 3445–3452.
- [57] G. Zanetti, C.H. Williams Jr., Characterization of the active center of thioredoxin reductase, J. Biol. Chem. 242 (22) (1967) 5232–5236.
- [58] L. Thelander, Studies on thioredoxin reductase from Escherichia coli B. The relation of structure and function, Eur. J. Biochem. 4 (3) (1968) 407–419.
- [59] B.W. Lennon, C.H. Williams Jr., Reductive half-reaction of thioredoxin reductase from Escherichia coli, Biochemistry 36 (31) (1997) 9464–9477.
- [60] B.W. Lennon, C.H. Williams Jr., Enzyme-monitored turnover of Escherichia coli thioredoxin reductase: insights for catalysis, Biochemistry 35 (15) (1996) 4704–4712.
- [61] L.B. Poole, C.M. Reynolds, Z.A. Wood, P.A. Karplus, H.R. Ellis, M. Li Calzi, AhpF and other NADH:peroxiredoxin oxidoreductases, homologues of low Mr thioredoxin reductase, Eur. J. Biochem. 267 (20) (2000) 6126–6133.
- [62] L. Chen, Q.W. Xie, C. Nathan, Alkyl hydroperoxide reductase subunit C (AhpC) protects bacterial and human cells against reactive nitrogen intermediates, Mol. Cell 1 (6) (1998) 795–805.
- [63] H.R. Ellis, L.B. Poole, Roles for the two cysteine residues of AhpC in catalysis of peroxide reduction by alkyl hydroperoxide reductase from Salmonella typhimurium, Biochemistry 36 (43) (1997) 13349–13356.
- [64] Y. Niimura, L.B. Poole, V. Massey, Amphibacillus xylanus NADH oxidase and Salmonella typhimurium alkyl-hydroperoxide reductase flavoprotein components show extremely high scavenging activity for both alkyl hydroperoxide and hydrogen peroxide in the presence of S. typhimurium alkyl-hydroperoxide reductase 22-kDa protein component, J. Biol. Chem. 270 (43) (1995) 25645–25650.
- [65] L.C. Seaver, J.A. Imlay, Alkyl hydroperoxide reductase is the primary scavenger of endogenous hydrogen peroxide in Escherichia coli, J. Bacteriol. 183 (24) (2001) 7173–7181.
- [66] G. Storz, F.S. Jacobson, L.A. Tartaglia, R.W. Morgan, L.A. Silveira, B.N. Ames, An alkyl hydroperoxide reductase induced by oxidative stress in Salmonella typhimurium and Escherichia coli: genetic characterization and cloning of ahp, J. Bacteriol. 171 (4) (1989) 2049–2055.
- [67] F.S. Jacobson, R.W. Morgan, M.F. Christman, B.N. Ames, An alkyl hydroperoxide reductase from Salmonella typhimurium involved in the defense of DNA against oxidative damage. Purification and properties, J. Biol. Chem. 264 (3) (1989) 1488–1496
- [68] M.F. Christman, R.W. Morgan, F.S. Jacobson, B.N. Ames, Positive control of a regulon for defenses against oxidative stress and some heat-shock proteins in Salmonella typhimurium, Cell 41 (3) (1985) 753–762.
- [69] L.A. Tartaglia, G. Storz, M.H. Brodsky, A. Lai, B.N. Ames, Alkyl hydroperoxide reductase from Salmonella typhimurium. Sequence and homology to thioredoxin reductase and other flavoprotein disulfide oxidoreductases, J. Biol. Chem. 265 (18) (1990) 10535–10540.
- [70] Z.A. Wood, L.B. Poole, P.A. Karplus, Structure of intact AhpF reveals a mirrored thioredoxin-like active site and implies large domain rotations during catalysis, Biochemistry 40 (13) (2001) 3900–3911.
- [71] P.V. Dip, N. Kamariah, M.S. Subramanian Manimekalai, W. Nartey, A. M. Balakrishna, F. Eisenhaber, B. Eisenhaber, G. Gruber, Structure, mechanism and ensemble formation of the alkylhydroperoxide reductase subunits AhpC and AhpF from Escherichia coli, Acta Crystallogr. D Biol. Crystallogr. 70 (Pt 11) (2014) 2848–2862.
- [72] N. Kamariah, M.S. Manimekalai, W. Nartey, F. Eisenhaber, B. Eisenhaber, G. Gruber, Crystallographic and solution studies of NAD(+)- and NADH-bound alkylhydroperoxide reductase subunit F (AhpF) from Escherichia coli provide insight into sequential enzymatic steps, Biochim. Biophys. Acta 1847 (10) (2015) 1139–1152.
- [73] T.J. Jonsson, H.R. Ellis, L.B. Poole, Cysteine reactivity and thiol-disulfide interchange pathways in AhpF and AhpC of the bacterial alkyl hydroperoxide reductase system, Biochemistry 46 (19) (2007) 5709–5721.
- [74] K. Ohnishi, Y. Niimura, K. Yokoyama, M. Hidaka, H. Masaki, T. Uchimura, H. Suzuki, T. Uozumi, M. Kozaki, K. Komagata, T. Nishino, et al., Purification and analysis of a flavoprotein functional as NADH oxidase from Amphibacillus xylanus overexpressed in Escherichia coli, J. Biol. Chem. 269 (50) (1994) 31418–31423.

- [75] Y. Niimura, V. Massey, Reaction mechanism of Amphibacillus xylanus NADH oxidase/alkyl hydroperoxide reductase flavoprotein, J. Biol. Chem. 271 (48) (1996) 30459–30464.
- [76] M. Li Calzi, L.B. Poole, Requirement for the two AhpF cystine disulfide centers in catalysis of peroxide reduction by alkyl hydroperoxide reductase, Biochemistry 36 (43) (1997) 13357–13364.
- [77] C.M. Reynolds, L.B. Poole, Attachment of the N-terminal domain of Salmonella typhimurium AhpF to Escherichia coli thioredoxin reductase confers AhpC reductase activity but does not affect thioredoxin reductase activity, Biochemistry 39 (30) (2000) 8859–8869.
- [78] L.B. Poole, A. Godzik, A. Nayeem, J.D. Schmitt, AhpF can be dissected into two functional units: tandem repeats of two thioredoxin-like folds in the N-terminus mediate electron transfer from the thioredoxin reductase-like C-terminus to AhpC, Biochemistry 39 (22) (2000) 6602–6615.
- [79] N.E. Engstrom, A. Holmgren, A. Larsson, S. Soderhall, Isolation and characterization of calf liver thioredoxin, J. Biol. Chem. 249 (1) (1974) 205–210.
- [80] E.C. Moore, A thioredoxin-thioredoxin reductase system from rat tumor, Biochem. Biophys. Res. Commun. 29 (3) (1967) 264–268.
- [81] M. Luthman, A. Holmgren, Rat liver thioredoxin and thioredoxin reductase: purification and characterization, Biochemistry 21 (26) (1982) 6628–6633.
- [82] H. Bauer, S. Gromer, A. Urbani, M. Schnolzer, R.H. Schirmer, H.M. Muller, Thioredoxin reductase from the malaria mosquito Anopheles gambiae, Eur. J. Biochem. 270 (21) (2003) 4272–4281.
- [83] T.W. Gilberger, R.D. Walter, S. Muller, Identification and characterization of the functional amino acids at the active site of the large thioredoxin reductase from Plasmodium falciparum, J. Biol. Chem. 272 (47) (1997) 29584–29589.
- [84] A.A. Turanov, D. Su, V.N. Gladyshev, Characterization of alternative cytosolic forms and cellular targets of mouse mitochondrial thioredoxin reductase, J. Biol. Chem. 281 (32) (2006) 22953–22963.
- [85] Q.A. Sun, Y. Wu, F. Zappacosta, K.T. Jeang, B.J. Lee, D.L. Hatfield, V. N. Gladyshev, Redox regulation of cell signaling by selenocysteine in mammalian thioredoxin reductases, J. Biol. Chem. 274 (35) (1999) 24522–24530.
- [86] J. Lu, L. Zhong, M.E. Lonn, R.F. Burk, K.E. Hill, A. Holmgren, Penultimate selenocysteine residue replaced by cysteine in thioredoxin reductase from selenium-deficient rat liver, Faseb. J. 23 (8) (2009) 2394–2402.
- [87] D. Mustacich, G. Powis, Thioredoxin reductase, Biochem. J. 346 (Pt 1) (2000) 1–8, Pt 1.
- [88] P.A. Karplus, G.E. Schulz, Substrate binding and catalysis by glutathione reductase as derived from refined enzyme: substrate crystal structures at 2 A resolution, J. Mol. Biol. 210 (1) (1989) 163–180.
- [89] K. Fritz-Wolf, S. Urig, K. Becker, The structure of human thioredoxin reductase 1 provides insights into C-terminal rearrangements during catalysis, J. Mol. Biol. 370 (1) (2007) 116–127.
- [90] T. Sandalova, L. Zhong, Y. Lindqvist, A. Holmgren, G. Schneider, Three-dimensional structure of a mammalian thioredoxin reductase: implications for mechanism and evolution of a selenocysteine-dependent enzyme, Proc. Natl. Acad. Sci. U. S. A. 98 (17) (2001) 9533–9538.
- [91] P.Y. Gasdaska, J.R. Gasdaska, S. Cochran, G. Powis, Cloning and sequencing of a human thioredoxin reductase, FEBS Lett. 373 (1) (1995) 5–9.
- [92] K. Fritz-Wolf, E. Jortzik, M. Stumpf, J. Preuss, R. Iozef, S. Rahlfs, K. Becker, Crystal structure of the Plasmodium falciparum thioredoxin reductasethioredoxin complex, J. Mol. Biol. 425 (18) (2013) 3446–3460.
- [93] K. Fritz-Wolf, S. Kehr, M. Stumpf, S. Rahlfs, K. Becker, Crystal structure of the human thioredoxin reductase-thioredoxin complex, Nat. Commun. 2 (2011) 383.
- [94] L. Zhong, E.S. Arner, A. Holmgren, Structure and mechanism of mammalian thioredoxin reductase: the active site is a redox-active selenolthiol/ selenenylsulfide formed from the conserved cysteine-selenocysteine sequence, Proc. Natl. Acad. Sci. U. S. A. 97 (11) (2000) 5854–5859.
- [95] L.D. Arscott, S. Gromer, R.H. Schirmer, K. Becker, C.H. Williams Jr., The mechanism of thioredoxin reductase from human placenta is similar to the mechanisms of lipoamide dehydrogenase and glutathione reductase and is distinct from the mechanism of thioredoxin reductase from Escherichia coli, Proc. Natl. Acad. Sci. U. S. A. 94 (8) (1997) 3621–3626.
- [96] P.F. Wang, L.D. Arscott, T.W. Gilberger, S. Muller, C.H. Williams Jr., Thioredoxin reductase from Plasmodium falciparum: evidence for interaction between the Cterminal cysteine residues and the active site disulfide-dithiol, Biochemistry 38 (10) (1999) 3187–3196.
- [97] T.W. Gilberger, B. Bergmann, R.D. Walter, S. Muller, The role of the C-terminus for catalysis of the large thioredoxin reductase from Plasmodium falciparum, FEBS Lett. 425 (3) (1998) 407–410.
- [98] G. Boumis, G. Giardina, F. Angelucci, A. Bellelli, M. Brunori, D. Dimastrogiovanni, F. Saccoccia, A.E. Miele, Crystal structure of Plasmodium falciparum thioredoxin reductase, a validated drug target, Biochem. Biophys. Res. Commun. 425 (4) (2012) 806–811.
- [99] L. Zhong, A. Holmgren, Essential role of selenium in the catalytic activities of mammalian thioredoxin reductase revealed by characterization of recombinant enzymes with selenocysteine mutations, J. Biol. Chem. 275 (24) (2000) 18121–18128.
- [100] B. Fox, C.T. Walsh, Mercuric reductase. Purification and characterization of a transposon-encoded flavoprotein containing an oxidation-reduction-active disulfide, J. Biol. Chem. 257 (5) (1982) 2498–2503.
- [101] T.K. Misra, N.L. Brown, D.C. Fritzinger, R.D. Pridmore, W.M. Barnes, L. Haberstroh, S. Silver, Mercuric ion-resistance operons of plasmid R100 and transposon Tn501: the beginning of the operon including the regulatory region and the first two structural genes, Proc. Natl. Acad. Sci. U. S. A. 81 (19) (1984) 5975–5979.

- [102] T. Barkay, S.M. Miller, A.O. Summers, Bacterial mercury resistance from atoms to ecosystems, FEMS Microbiol. Rev. 27 (2–3) (2003) 355–384.
- [103] M.D.D. Melissa J. Moore, Lynne D. Zydowsky, Richard T. Cummings, Christopher T. Walsh, Organomercurial lyase and mercuric ion reductase: nature's mercury detoxification catalyst, Acc. Chem. Res. 23 (9) (1990) 301–308.
- [104] A.O. Summers, S. Silver, Mercury resistance in a plasmid-bearing strain of Escherichia coli, J. Bacteriol. 112 (3) (1972) 1228–1236.
- [105] J. Schottel, A. Mandal, D. Clark, S. Silver, R.W. Hedges, Volatilisation of mercury and organomercurials determined by inducible R-factor systems in enteric bacteria, Nature 251 (5473) (1974) 335–337.
- [106] D.L. Clark, A.A. Weiss, S. Silver, Mercury and organomercurial resistances determined by plasmids in Pseudomonas, J. Bacteriol. 132 (1) (1977) 186–196.
- [107] B.S. Fox, C.T. Walsh, Mercuric reductase: homology to glutathione reductase and lipoamide dehydrogenase. Iodoacetamide alkylation and sequence of the active site peptide, Biochemistry 22 (17) (1983) 4082–4088.
- [108] N.L. Brown, S.J. Ford, R.D. Pridmore, D.C. Fritzinger, Nucleotide sequence of a gene from the Pseudomonas transposon Tn501 encoding mercuric reductase, Biochemistry 22 (17) (1983) 4089–4095.
- [109] S.M. Miller, D.P. Ballou, V. Massey, C.H. Williams Jr., C.T. Walsh, Two-electron reduced mercuric reductase binds Hg(II) to the active site dithiol but does not catalyze Hg(II) reduction, J. Biol. Chem. 261 (18) (1986) 8081–8084.
- [110] S.M. Miller, M.J. Moore, V. Massey, C.H. Williams Jr., M.D. Distefano, D. P. Ballou, C.T. Walsh, Evidence for the participation of Cys558 and Cys559 at the active site of mercuric reductase, Biochemistry 28 (3) (1989) 1194–1205.
- [111] M.D. Distefano, K.G. Au, C.T. Walsh, Mutagenesis of the redox-active disulfide in mercuric ion reductase: catalysis by mutant enzymes restricted to flavin redox chemistry, Biochemistry 28 (3) (1989) 1168–1183.
- [112] M.J. Moore, C.T. Walsh, Mutagenesis of the N- and C-terminal cysteine pairs of Tn501 mercuric ion reductase: consequences for bacterial detoxification of mercurials, Biochemistry 28 (3) (1989) 1183–1194.
- [113] S.M. Miller, V. Massey, D. Ballou, C.H. Williams Jr., M.D. Distefano, M.J. Moore, C.T. Walsh, Use of a site-directed triple mutant to trap intermediates: demonstration that the flavin C(4a)-thiol adduct and reduced flavin are kinetically competent intermediates in mercuric ion reductase, Biochemistry 29 (11) (1990) 2831–2841.
- [114] N.L. Brown, Bacterial resistance to mercury reductio ad absurdum, Trends Biochem. Sci. 10 (10) (1985) 400–403.
- [115] R. Ledwidge, B. Patel, A. Dong, D. Fiedler, M. Falkowski, J. Zelikova, A. O. Summers, E.F. Pai, S.M. Miller, NmerA, the metal binding domain of mercuric ion reductase, removes Hg2+ from proteins, delivers it to the catalytic core, and protects cells under glutathione-depleted conditions, Biochemistry 44 (34) (2005) 11402–11416.
- [116] A. Johs, I.M. Harwood, J.M. Parks, R.E. Nauss, J.C. Smith, L. Liang, S.M. Miller, Structural characterization of intramolecular Hg(2+) transfer between flexibly linked domains of mercuric ion reductase, J. Mol. Biol. 413 (3) (2011) 639–656.
- [117] D. Rennex, R.T. Cummings, M. Pickett, C.T. Walsh, M. Bradley, Role of tyrosine residues in Hg(II) detoxification by mercuric reductase from Bacillus sp. strain RC607, Biochemistry 32 (29) (1993) 7475–7478.
- [118] S. Engst, S.M. Miller, Rapid reduction of Hg(II) by mercuric ion reductase does not require the conserved C-terminal cysteine pair using HgBr2 as the substrate, Biochemistry 37 (33) (1998) 11496–11507.
- [119] S. Engst, S.M. Miller, Alternative routes for entry of HgX2 into the active site of mercuric ion reductase depend on the nature of the X ligands, Biochemistry 38 (12) (1999) 3519–3529.
- [120] L. Sahlman, A.M. Lambeir, S. Lindskog, Rapid-scan stopped-flow studies of the pH dependence of the reaction between mercuric reductase and NADPH, Eur. J. Biochem. 156 (3) (1986) 479–488.
- [121] Q.A. Sun, L. Kirnarsky, S. Sherman, V.N. Gladyshev, Selenoprotein oxidoreductase with specificity for thioredoxin and glutathione systems, Proc. Natl. Acad. Sci. U. S. A. 98 (7) (2001) 3673–3678.
- [122] H.M. Alger, D.L. Williams, The disulfide redox system of Schistosoma mansoni and the importance of a multifunctional enzyme, thioredoxin glutathione reductase, Mol. Biochem. Parasitol. 121 (1) (2002) 129–139.
- [123] G. Salinas, M.E. Selkirk, C. Chalar, R.M. Maizels, C. Fernandez, Linked thioredoxin-glutathione systems in platyhelminths, Trends Parasitol. 20 (7) (2004) 340–346.
- [124] A. Agorio, C. Chalar, S. Cardozo, G. Salinas, Alternative mRNAs arising from trans-splicing code for mitochondrial and cytosolic variants of Echinococcus granulosus thioredoxin Glutathione reductase, J. Biol. Chem. 278 (15) (2003) 12920–12928.
- [125] J.L. Rendon, I.P. del Arenal, A. Guevara-Flores, A. Uribe, A. Plancarte, G. Mendoza-Hernandez, Purification, characterization and kinetic properties of the multifunctional thioredoxin-glutathione reductase from Taenia crassiceps metacestode (cysticerci), Mol. Biochem. Parasitol. 133 (1) (2004) 61–69.
- [126] A. Guevara-Flores, J.P. Pardo, J.L. Rendon, Hysteresis in thioredoxin-glutathione reductase (TGR) from the adult stage of the liver fluke Fasciola hepatica, Parasitol. Int. 60 (2) (2011) 156–160.
- [127] D.L. Williams, M. Bonilla, V.N. Gladyshev, G. Salinas, Thioredoxin glutathione reductase-dependent redox networks in platyhelminth parasites, Antioxidants Redox Signal. 19 (7) (2013) 735–745.
- [128] A.N. Kuntz, E. Davioud-Charvet, A.A. Sayed, L.L. Califf, J. Dessolin, E.S. Arner, D. L. Williams, Thioredoxin glutathione reductase from Schistosoma mansoni: an essential parasite enzyme and a key drug target, PLoS Med. 4 (6) (2007) e206.
- [129] J.J. Martinez-Gonzalez, A. Guevara-Flores, G. Alvarez, J.L. Rendon-Gomez, I. P. Del Arenal, In vitro killing action of auranofin on Taenia crassiceps

- metacestode (cysticerci) and inactivation of thioredoxin-glutathione reductase (TGR), Parasitol. Res. 107 (1) (2010) 227–231.
- [130] S.K. Park, L. Friedrich, N.A. Yahya, C.M. Rohr, E.G. Chulkov, D. Maillard, F. Rippmann, T. Spangenberg, J.S. Marchant, Mechanism of praziquantel action at a parasitic flatworm ion channel, Sci. Transl. Med. 13 (625) (2021) eabj5832.
- [131] A.A. Sayed, A. Simeonov, C.J. Thomas, J. Inglese, C.P. Austin, D.L. Williams, Identification of oxadiazoles as new drug leads for the control of schistosomiasis, Nat. Med. 14 (4) (2008) 407–412.
- [132] F. Angelucci, A.A. Sayed, D.L. Williams, G. Boumis, M. Brunori, D. Dimastrogiovanni, A.E. Miele, F. Pauly, A. Bellelli, Inhibition of Schistosoma mansoni thioredoxin-glutathione reductase by auranofin: structural and kinetic aspects, J. Biol. Chem. 284 (42) (2009) 28977–28985.
- [133] U.H. Park, H.S. Han, E. Um, X.H. An, E.J. Kim, S.J. Um, Redox regulation of transcriptional activity of retinoic acid receptor by thioredoxin glutathione reductase (TGR), Biochem. Biophys. Res. Commun. 390 (2) (2009) 241–246.
- [134] D. Su, S.V. Novoselov, Q.A. Sun, M.E. Moustafa, Y. Zhou, R. Oko, D.L. Hatfield, V. N. Gladyshev, Mammalian selenoprotein thioredoxin-glutathione reductase. Roles in disulfide bond formation and sperm maturation, J. Biol. Chem. 280 (28) (2005) 26491–26498.
- [135] F.T. Ogata, V. Branco, F.F. Vale, L. Coppo, Glutaredoxin: discovery, redox defense and much more, Redox Biol. 43 (2021) 101975.
- [136] F. Angelucci, A.E. Miele, G. Boumis, D. Dimastrogiovanni, M. Brunori, A. Bellelli, Glutathione reductase and thioredoxin reductase at the crossroad: the structure of Schistosoma mansoni thioredoxin glutathione reductase, Proteins 72 (3) (2008) 036-045
- [137] I. Silvestri, H. Lyu, F. Fata, G. Boumis, A.E. Miele, M. Ardini, R. Ippoliti, A. Bellelli, A. Jadhav, W.A. Lea, A. Simeonov, Q. Cheng, E.S.J. Arner, G.R. J. Thatcher, P.A. Petukhov, D.L. Williams, F. Angelucci, Fragment-based discovery of a regulatory site in thioredoxin glutathione reductase acting as "doorstop" for NADPH entry, ACS Chem. Biol. 13 (8) (2018) 2190–2202.
- [138] V.Z. Petukhova, S.Y. Aboagye, M. Ardini, R.P. Lullo, F. Fata, M.E. Byrne, F. Gabriele, L.M. Martin, L.N.M. Harding, V. Gone, B. Dangi, D.D. Lantvit, D. Nikolic, R. Ippoliti, G. Effantin, W.L. Ling, J.J. Johnson, G.R.J. Thatcher, F. Angelucci, D.L. Williams, P.A. Petukhov, Non-covalent inhibitors of

- thioredoxin glutathione reductase with schistosomicidal activity in vivo, Nat. Commun. 14 (1) (2023) 3737.
- [139] F. Fata, I. Silvestri, M. Ardini, R. Ippoliti, L. Di Leandro, N. Demitri, M. Polentarutti, A. Di Matteo, H. Lyu, G.R.J. Thatcher, P.A. Petukhov, D. L. Williams, F. Angelucci, Probing the surface of a parasite drug target thioredoxin glutathione reductase using small molecule fragments, ACS Infect. Dis. 7 (7) (2021) 1932–1944.
- [140] M. Bonilla, A. Denicola, S.V. Novoselov, A.A. Turanov, A. Protasio, D. Izmendi, V. N. Gladyshev, G. Salinas, Platyhelminth mitochondrial and cytosolic redox homeostasis is controlled by a single thioredoxin glutathione reductase and dependent on selenium and glutathione, J. Biol. Chem. 283 (26) (2008) 17898–17007
- [141] M. Bonilla, A. Denicola, S.M. Marino, V.N. Gladyshev, G. Salinas, Linked thioredoxin-glutathione systems in platyhelminth parasites: alternative pathways for glutathione reduction and deglutathionylation, J. Biol. Chem. 286 (7) (2011) 4959–4967.
- [142] H.H. Huang, L. Day, C.L. Cass, D.P. Ballou, C.H. Williams Jr., D.L. Williams, Investigations of the catalytic mechanism of thioredoxin glutathione reductase from Schistosoma mansoni, Biochemistry 50 (26) (2011) 5870–5882.
- [143] Q.A. Sun, D. Su, S.V. Novoselov, B.A. Carlson, D.L. Hatfield, V.N. Gladyshev, Reaction mechanism and regulation of mammalian thioredoxin/glutathione reductase, Biochemistry 44 (44) (2005) 14528–14537.
- [144] C. Brandstaedter, K. Fritz-Wolf, S. Weder, M. Fischer, B. Hecker, S. Rahlfs, K. Becker, Kinetic characterization of wild-type and mutant human thioredoxin glutathione reductase defines its reaction and regulatory mechanisms, FEBS J. 285 (3) (2018) 542–558.
- [145] M.M. Smith, T.B. Alt, D.L. Williams, G.R. Moran, Descriptive analysis of transientstate observations for thioredoxin/glutathione reductase (Sec597Cys) from schistosoma mansoni, Biochemistry 62 (9) (2023) 1497–1508.
- [146] A. Holmgren, Thioredoxin catalyzes the reduction of insulin disulfides by dithiothreitol and dihydrolipoamide, J. Biol. Chem. 254 (19) (1979) 9627–9632.
- [147] M.M. Smith, G.R. Moran, Assigning function to active site residues of Schistosoma mansoni thioredoxin/glutathione reductase from analysis of transient state reductive half-reactions with variant forms of the enzyme, Front. Mol. Biosci. 10 (2023) 1258333.